



Published in final edited form as:

Nature. 2018 October ; 562(7728): 526–531. doi:10.1038/s41586-018-0623-z.

## Functional Genomic Landscape of Acute Myeloid Leukemia

*A full list of authors and affiliations appears at the end of the article.*

### Abstract

The implementation of targeted therapies for acute myeloid leukemia has been challenged by complex mutational patterns within and across patients as well as a dearth of pharmacologic agents for most mutational events. Here, we report initial findings from the Beat AML program on a cohort of 672 tumor specimens collected from 562 patients. We assessed these specimens using whole exome sequencing, RNA-sequencing, and *ex vivo* drug sensitivity analyses. Our data reveal

Users may view, print, copy, and download text and data-mine the content in such documents, for the purposes of academic research, subject always to the full Conditions of use:[http://www.nature.com/authors/editorial\\_policies/license.html#terms](http://www.nature.com/authors/editorial_policies/license.html#terms) Reprints and permissions information is available at [www.nature.com/reprints](http://www.nature.com/reprints). Readers are welcome to comment on the online version of the paper.

Correspondence and requests for materials should be addressed to SKM ([mcweeney@ohsu.edu](mailto:mcweeney@ohsu.edu)) or BJD ([drukerb@ohsu.edu](mailto:drukerb@ohsu.edu)).

Contact Shannon McWeeney, [mcweeney@ohsu.edu](mailto:mcweeney@ohsu.edu), Brian Druker, [drukerb@ohsu.edu](mailto:drukerb@ohsu.edu)

**Author Contributions** JWT, CET, DB, BW, SEK, SLS, NL, ARS, ET, SKM, and BJD contributed equally to this work. JWT, CET, SKM, AA, and BJD provided project oversight for experimental design, data management, data analysis and Interpretation, methods development, and development of Vizome platform; BW assisted in the development of Vizome platform, project oversight for experimental design, workflow development, data processing, management, analysis and dissemination, and methods development; ET provided patient sample acquisition, clinical data structure, collection, and analysis; SS, AR-S, MA, IE, AR assisted in patient sample processing, *ex vivo* drug screening, DNA/RNA extractions and sequencing sample submissions; NL, R, JD, CV provided curation and entry of patient clinical annotations; SK provided variant confirmation, and data analysis; DB assisted in workflow development for pre-processing and analysis of RNA-seq, Exome-Seq and Ex Vivo Drug Screening, RNA-seq, clinical data curation and integration, methods development, multivariate modeling and Integration, and development of Vizome platform; JR, RS, AY provided clinical data integration from OHSU Research Data Warehouse; TK assisted in recruiting patients and harvesting samples for analysis; CRC, RTS were co-Investigators for the repository protocol, edited and provided feedback on manuscript; CTJ, DAP collected samples for repository protocol, provided feedback on manuscript; MEM, RRP consented patients and collected samples for the repository protocol and aided with clinical annotation; DN assisted in the creation of drug screening replicate plates; CAE, KW-S, HZ assisted in data analysis; DKE provided data analysis, data curation, and development of analytical processes; AK, TM assisted in the development of the *ex vivo* drug screening processing workflow; SJW enabled, facilitated and mentored basic, translational and clinical research activities arising from data generated by Beat AML at the University of Kansas Cancer Center site, participated in the Beat AML Symposia to share research and create new research projects; ES, AC, RH, CL, RS provided exome and RNA-Seq library creation, sequencing, and data processing; DD, CN, JP assisted in genomic isolation, curation of samples and entry of patient clinical annotations; DLW served as a Liaison for sample acquisition; MWD served as a Local Principal Investigator for repository protocol, consented patients and collected samples for repository protocol, aided with clinical annotation, edited and provided feedback on manuscript; RLW served as a manager for their repository protocol, consented patients and collected samples for the repository, aided with clinical annotation, edited and provided feedback on manuscript; MML assisted in patient sample acquisition, IRB protocol development and maintenance, clinical data structure, collection, and analysis; UM, BHC, RC, AD, K-HD, JL, SEP assisted in patient sample acquisition; JB, RB, CC, MD, JG, HH, AJ, KJ, RJ, SL, SL, JMac, JMar, RS, TS, AT, JWa, JWo provided patient sample processing and *ex vivo* drug screening; CSH served as Principal Investigator for their local protocol; consented patients and collected samples for repository protocol, aided with clinical annotation, edited and provided feedback on manuscript; JMW served as Principal Investigator for their local repository protocol, edited and provided feedback on manuscript; BCM served as Principal Investigator for their local repository protocol, consented patients and collected samples for repository protocol, aided with clinical annotation, edited and provided feedback on manuscript; DCC, TLL, RHC served as Principal Investigators for their local repository protocol, consented patients and collected samples for repository protocol, aided with clinical annotation, edited and provided feedback on manuscript; TM provided regulatory oversight; BJ, KW provided regulatory oversight, curation and entry of patient clinical annotations; AB provided targetome overlay; JC, CO assisted in tech transfer, and project development.

#### Data Availability Statement

All raw and processed sequencing data, along with relevant clinical annotations have been submitted to dbGaP and Genomic Data Commons. The dbGaP study ID is 30641 and accession ID is phs001657.v1.p1. The raw data for clinical annotations, variant calls, gene expression counts, and drug sensitivity that underlie all figures in this manuscript are found in the Supplementary Information. In addition, all data can be accessed and queried through our online, interactive user interface, Vizome, at [www.vizome.org](http://www.vizome.org).

Supplementary Information is available in the online version of the paper.

See also Supplementary Information for listing of authors, affiliations, and contributions

novel mutational events not previously detected in AML. We show association of drug response with mutational status, including instances of drug sensitivity that are specific to combinatorial mutational events. Integration with RNA-sequencing also revealed gene expression signatures, which predict a role of specific gene networks in drug response. Collectively, this report offers a dataset, accessible by the Beat AML data viewer ([www.vizome.org](http://www.vizome.org)), that can be leveraged to address clinical, genomic, transcriptomic, and functional inquiries into the biology of AML.

## INTRODUCTION

Approximately 21,000 people are diagnosed with acute myeloid leukemia (AML) with over 10,000 AML-related deaths annually in the United States<sup>1,2</sup>. Cytogenetic and sequencing analyses have revealed at least 11 genetic classes of AML<sup>3</sup> and over 20 subsets can be assigned when also considering cell differentiation states of the leukemic blasts<sup>4,5</sup>. Deep sequencing of AML by The Cancer Genome Atlas (TCGA) revealed a heterogeneous disease with nearly 2,000 somatically mutated genes observed across 200 patients<sup>6</sup>. Many of the recurrent cytogenetic events and somatic mutations have been shown to carry prognostic significance<sup>3,7,8</sup>. Some of the most frequent somatic variants can also be observed in myelodysplastic syndromes (MDS) and myeloproliferative neoplasms (MPN)<sup>9–11</sup> that can transform into AML. These same mutations have also been observed in healthy individuals exhibiting age-related clonal hematopoiesis, which carries significant risk for the development of MDS, MPN, and AML<sup>12–15</sup>.

A small number of therapies targeted to mutational events have been developed for AML patients, with the current standard of care largely unchanged over the past 30–40 years. The first targeted therapy for AML involved use of all-trans retinoic acid (ATRA) in combination with arsenic trioxide for patients with rearrangement of the retinoic acid receptor<sup>16,17</sup>. More recently, fms related tyrosine kinase 3 (FLT3) inhibitors have been developed for FLT3 mutational events that occur in ~20–30% of AML patients<sup>18–21</sup>. FLT3 inhibitors deployed as single agents yielded responses of only 2–6 months<sup>22–25</sup>. Midostaurin, a broad-spectrum FLT3 inhibitor, was recently approved for use in newly diagnosed, FLT3-mutated AML patients in combination with standard of care chemotherapy<sup>26</sup>; however, relapse was still prevalent in this setting. Targeting of mutant isocitrate dehydrogenase (NADP(+)) 1, cytosolic 1/2 (IDH1/2)<sup>27</sup>, has shown clinical benefit leading to approval of the IDH2 inhibitor, enasidenib, and the IDH1 inhibitor, ivosidenib<sup>28,29</sup>. Additional proposed strategies have included inhibition of epigenetic modifiers such as enhancer of zeste 2 polycomb repressive complex 2 subunit (EZH2)<sup>30</sup>, LSD1 zinc finger family protein (LSD1)<sup>31</sup>, and DOT1L like histone lysine methyltransferase (DOT1L)<sup>32</sup> based on direct mutation of these targets or synthetic lethality in the context of drug combinations (ATRA and LSD1 inhibitors) or specific genetic features (lysine methyltransferase 2A (*KMT2A*)-gene rearrangement for DOT1L inhibitors). Hypomethylating agents have been employed in AML patients with better responses reported for certain genetic subsets, such as those with mutation of TET2<sup>33</sup> or tumor protein 53 (TP53)<sup>34</sup>. Most recently, the BCL2 apoptosis regulator (BCL2) inhibitor, venetoclax, showed a ~20% response rate when used as a single agent in relapsed patients<sup>35</sup> with higher response rates (~60%) reported in combination with hypomethylating agents in newly diagnosed, elderly AML patients<sup>36</sup>.

## RESULTS

To better understand genetic or transcriptional markers and mechanisms of drug sensitivity and resistance in AML, we developed a cohort of 672 primary specimens from 562 unique AML patients on which extensive functional and genomic interrogations were undertaken. Detailed clinical annotations, including diagnostic information, clinical laboratory values, treatments, responses and outcomes were curated from electronic medical records and are reported in Supplementary Information (Tables S1–5).

### Comparative Genomic Landscape of AML

We performed exome sequencing on 622 of the specimens from the cohort representing 531 unique patients. The final, high-confidence variant list (Supplementary Information, Table S7) revealed a range of 1–80 somatic variants per patient (cohort median of 13 somatic variants) (Extended Data Fig. 1). Comparison of the top 33 most commonly mutated genes across Beat AML and TCGA<sup>6</sup> showed generally similar frequencies. Higher frequency of mutations in serine and arginine rich splicing factor 2 (SRSF2) were seen in Beat AML than in TCGA, and this difference was conserved comparing only the *de novo* cases in Beat AML with TCGA (Fig. 1A). In contrast, mutational events that were seen at less than 2% frequency across Beat AML and TCGA were much more divergent with variants in 221 mutant genes called in common, 939 mutant genes called only in TCGA, and ~1,500 mutant genes called only in Beat AML, irrespective of whether we compared only *de novo* or non-*de novo* cases (Fig. 1B,C). Most of these divergent mutational events were observed in only single patients, however, there were mutations in 11 genes that were called in 1% or more of patients in Beat AML, but were not observed in prior AML sequencing studies (Extended Data Fig. 1). Finally, co-occurrence and exclusivity of the most frequent variants were computed revealing significant patterns of mutational co-segregation suggesting biological cooperativity of certain mutational events (Fig. 1D).

### Drug Response and Gene Expression

RNA sequencing was performed on 451 specimens from 411 patients. Clustering of the 2,000 most variably expressed genes across the cohort revealed gene expression signatures that associated with many of the prominent genetic and cytogenetic disease groups (Extended Data Fig. 2). To understand the profile of sensitivity and resistance to a variety of small-molecule inhibitors, we profiled primary tumor cells from 409 specimens derived from 363 patients against a panel of 122 small-molecule inhibitors using an *ex vivo* drug sensitivity assay<sup>37</sup>. Drug sensitivity patterns were analyzed with respect to clinical and genetic features of tumors (Extended Data Fig. 3). We compared the average area-under-the curve (AUC) values for each drug between the *de novo* and transformed samples via a series of single factor analysis of variance (ANOVA) tests. Generally, transformed cases showed less sensitivity to most drugs than *de novo* cases. Of the 122 drugs tested, 64 were significantly (false discovery rate (FDR) < .1) more sensitive in the *de novo* samples, while only 1 drug Panobinostat (HDAC inhibitor) was significantly more sensitive in the transformed cases (Extended Data Fig. 4). In addition, we analyzed the concordance of drug sensitivity patterns with respect to predicted target gene, gene family, or pathway for each drug (drug assignments to target families found in Supplementary Information, Table S11).

This analysis revealed drug targets/families that were highly concordant amongst constituent members as well as drug families that were quite discordant (Extended Data Fig. 5). To create a global view of overall sensitivity or resistance of each case, we generated a heatmap of binary sensitive/resistant calls for each sample to each drug. We then annotated the sensitivity or resistance fraction of each case against European Leukemia Net (ELN) 2017 (Extended Data Fig. 6A) and World Health Organization (WHO) 2016 (Extended Data Fig. 6B) classifications.

### Gene Signatures of Drug Response

We performed a cohort analysis to assess correlation between drug sensitivity patterns and mutational events or gene expression levels. Correlation of drug sensitivity with mutational events was performed by assessing the range of sensitivity of cases with mutation of an individual gene (as well as co-occurring mutational events) versus cases with wild type sequence for that same gene. Broad summaries of full cohort results are displayed in Circos and Manhattan plots (Extended Data Fig. 7A, 8). Individual drug/mutation associations are displayed on a Volcano plot with the horizontal axis showing difference in drug sensitivity between mutant versus wild type and FDR-corrected significance values<sup>38</sup> plotted on the vertical axis (Fig. 2A). Some of the associations showing highest levels of statistical significance involved FLT3-ITD exhibiting sensitivity to FLT3 pathway inhibitors, which served as a proof-of-principle since FLT3 inhibitors are known to be more effective against FLT3-ITD AML. However, to reveal drug/mutation associations that were not biased by co-occurrence with FLT3-ITD, we also plotted the same analysis using only cases that were wild type for FLT3 (Extended Data Fig. 7B). We also created Volcano plots that were specific to each individual drug (versus all mutational events) and for each individual gene (versus all drugs tested). All Volcano plots can be found with interactive features in our online data browser ([www.vizome.org](http://www.vizome.org)) and ([http://vizome.org/additional\\_figures\\_BeatAML.html](http://vizome.org/additional_figures_BeatAML.html)).

Mutation of several genes, most notably TP53 or ASXL1 transcriptional regulator 1 (ASXL1), were shown to cause a broad pattern of drug resistance. Interestingly, a few drugs trended more sensitive to TP53 mutant cases, such as elesclamol, or ASXL1, such as panobinostat, hinting at candidates to explore for AML cases with these poor prognostic features. Mutation of NRAS proto-oncogene, GTPase (NRAS) or KRAS proto-oncogene, GTPase) KRAS also correlated largely with resistance to most drugs, though did show the predicted sensitivity to MAPK inhibitors. It was interesting to note a stronger association of NRAS than KRAS mutation with MAPK sensitivity. IDH2 mutation conferred sensitivity to a broad spectrum of drugs, while mutation of IDH1 conferred resistance to most drugs. Mutation of RUNX1 correlated with sensitivity to PIK3C/MTOR inhibitors, such as BEZ235, and to the multi-kinase vascular endothelial growth factor receptor (VEGFR) inhibitor, cediranib. Mutation of spliceosome components U2 small nuclear RNA auxiliary factor 1 (U2AF1) and zinc finger CCCH-type, RNA binding motif and serine/arginine rich 2 (ZRSR2) correlated with novel sensitivity to several drugs. The mechanisms underlying these latter sensitivity correlations (and many others in the dataset) merit further investigation. A significant association was seen between mutation of FLT3, NPM1, and DNMT3A with sensitivity to the FDA approved drug, ibrutinib. Since these mutations

exhibit a significant pattern of co-occurrence, we next examined every combination of single, double, or triple mutation of these genes with respect to ibrutinib. We observed that DNMT3A alone or DNMT3A/FLT3 double mutant cases were not significantly different than wild type, while cases with FLT3-ITD alone or any variation of NPM1 mutation (including cases with all three genes mutated) were significantly more sensitive than wild type (Fig. 2B). Ibrutinib is an inhibitor of BTK and TEC family kinases, although it can exhibit broad off-target effects when maintained in continuous culture with target cells. We noted that another kinase inhibitor with high specificity for spleen associated tyrosine kinase (SYK), entospletinib, showed a similarly significant pattern of sensitivity for cases with FLT3-ITD and NPM1 (Fig. 2B), potentially pointing to an operationally important target for this disease subset. Indeed, prior work has suggested SYK as an interacting target of FLT3-ITD in AML<sup>39</sup>. Finally, we wanted to perform an additional analysis that leveraged multiple inhibitors with common targets to see whether this approach could identify additional associations. We focused on correlation of the four selective Janus kinase (JAK) inhibitors on our drug panel (mometinib, ruxolitinib, tofacitinib, and JAK Inhibitor I) with mutation of BCL6 corepressor (BCOR) alone or co-mutation of BCOR with DNMT3A, RUNX1, or SRSF2. By plotting the average difference of each JAK inhibitor between mutant and wild type groups of these four mutational categories and performing a one-way ANOVA analysis of the four groups, we found that co-mutation of BCOR with RUNX1 correlated with increased sensitivity to all four JAK kinase inhibitors, while BCOR mutation alone or co-mutation of BCOR with DNMT3A or SRSF2 showed no difference in sensitivity to the JAK kinase inhibitors, although BCOR mutation alone did show sensitivity to alternative drugs, such as the tankyrase/WNT inhibitor, XAV-939, and the multi-kinase inhibitor, crizotinib (Fig. 2C). Collectively, these data suggest that JAK pathway dysregulation may represent a vulnerability within certain, specific combinatorial mutation settings and not in others.

We also performed an integration of drug sensitivity data with respect to patterns of gene expression, comparing the 20% of samples with lowest AUC versus the 20% with highest AUC and assessing the most differentially expressed genes between those sample sets. This analysis revealed significant (FDR < .05) expression signatures for 78 testable drugs on the panel (78/119 65.5%). As an example, the 20% most and least sensitive cases to ibrutinib could be clearly distinguished by an expression signature of 17 genes (Fig. 3; Extended Data Fig. 9). Expression signature heatmaps for each drug can be found in our online data browser ([http://vizome.org/additional\\_figures\\_BeatAML.html](http://vizome.org/additional_figures_BeatAML.html)).

Finally, to assess the joint contributions of both mutation and system-level co-expression patterns (based on de-novo network inference) in predicting drug response, multivariate modeling was performed. This integrated analysis allows us to move beyond the significant associations of single mutations (such as FLT3-ITD and NPM1). We performed a weighted correlation network analysis (WGCNA) analysis of RNA-sequencing data that identified 14 sets of genes where gene expression patterns showed significant clustering across the cohort (clusters contained both elevated and decreased gene expression events). We performed iterative regression modeling (lasso) to understand how strongly any mutational event or any of these 14 gene expression clusters correlated with sensitivity or resistance to any of the drugs on the panel. We identified numerous, novel co-occurrences of mutations and expression clusters that were associated with drug sensitivity or resistance, with co-



occurrences to ibrutinib shown as an example (Extended Data Fig. 9). For ibrutinib, these co-occurrences included a co-expression cluster of 345 genes (using a color labeling scheme and indicated as “turquoise”) that correlated with drug sensitivity and frequently co-occurred with FLT3-ITD, which also correlated with drug sensitivity. There was significant overlap between this “turquoise” gene expression cluster and the 17-gene signature in Figure 3 (indicated by the ratio of observed overlap to expected or representation factor: 13.6;  $P < 1.734e-04$ ). It is important to note that network analysis of this gene expression cluster highlighted enrichment for a number of immune-related pathways, which was not detected within the 17-gene signature (displayed at [http://vizome.org/additional\\_figures\\_BeatAML.html](http://vizome.org/additional_figures_BeatAML.html)). We also identified a 110-gene subnetwork (labeled as “magenta” in Figure 6C), which was associated with resistance to ibrutinib and was significantly associated with adverse ELN 2017 risk. To look more broadly at associations between mutations or gene expression clusters, we summarized drugs at family level to assess the frequency by which mutations and gene expression clusters were selected in iterative regression modeling (displayed at [http://vizome.org/additional\\_figures\\_BeatAML.html](http://vizome.org/additional_figures_BeatAML.html))

## DISCUSSION

In sum, here we report the largest functional genomic dataset of primary tumor biopsies to date. We present a cohort of AML patient specimens for which we have performed detailed clinical annotations, genomic and transcriptomic analyses, and *ex vivo* drug sensitivity studies, and we provide analytical approaches for data integration. Each of these datasets alone has revealed new information about the biology and potential translational approaches in AML, and the integration of these datasets has been revealing of new markers and mechanisms of drug sensitivity and resistance that merit further study. These data have all been made publicly available through the NIH/NCI dbGaP and Genomic Data Commons (GDC) resources, and we have developed tools to facilitate user interface with the dataset ([www.vizome.org](http://www.vizome.org)). We hope and expect that this public data release will stimulate further use of the data such that novel findings can be derived and parlayed into new clinical approaches for AML.

## METHODS

### Patient Samples

All patients gave informed consent to participate in this study, which had the approval and guidance of the institutional review boards at Oregon Health & Science University (OHSU), University of Utah, University of Texas Medical Center (UT Southwestern), Stanford University, University of Miami, University of Colorado, University of Florida, National Institutes of Health (NIH), Fox Chase Cancer Center and University of Kansas (KUMC). Samples were sent to the coordinating center (OHSU; IRB#9570; #4422; NCT01728402) where they were coded and processed. Specific names of centers associated with each specimen were coded and centers providing less than 5 samples were aggregated together and given one center identifier. Mononuclear cells were isolated by Ficoll gradient centrifugation from freshly obtained bone marrow aspirates or peripheral blood draws. Cell

pellets were snap frozen in liquid nitrogen for subsequent DNA isolation (Qiagen, DNeasy Blood & Tissue Kit), freshly pelleted cells were lysed immediately in guanidinium thiocyanate (GTC) lysate for subsequent RNA isolation (Qiagen, RNeasy Mini Kit), and freshly isolated mononuclear cells were plated into an *ex vivo* drug sensitivity assays within 24 hours (described in detail below). Skin punch biopsies were collected at the site of Jamshidi needle insertion for subsequent bone marrow biopsies and genomic DNA was isolated for use as matched normal controls for exome sequencing (Qiagen, DNeasy Blood & Tissue Kit). Clinical, prognostic, genetic, cytogenetic, and pathologic lab values as well as treatment and outcome data were manually curated from patient electronic medical records. Patients were assigned a specific diagnosis based on the prioritization of genetic and clinical factors as determined by WHO guidelines. To prevent re-identification, any patient over the age of 90 was placed into a >90 aggregated age bracket. Genetic characterization of the leukemia samples included results of a clinical deep-sequencing panel of genes commonly mutated in hematologic malignancies (Sequenome and GeneTrails (OHSU); Foundation Medicine (UTSW); Genoptix; and Illumina).

### Whole Exome and Custom Capture Validation Sequencing

For exome sequencing, Illumina Nextera RapidCapture Exome capture probes and protocol were utilized, which provided coverage of 37 Mb of genomic DNA coding regions. Briefly, following initial QC on a TapeStation (Agilent), 50 ng of intact genomic DNA was fragmented and tagged (tagmentation) in a single step. Following clean-up, the tagmented DNA was amplified by 10 cycles of PCR, which added the indexed adaptors for clustering and sequencing. Libraries were hybridized to capture pools in 12 sample sets with two rounds of hybridization performed to increase specificity. Libraries recovered with streptavidin magnetic beads were amplified by 10 cycles of PCR, unincorporated reagents were removed with AMPure beads (Agencourt), and validated on the TapeStation. Quantification of capture pools was done using real time PCR (Kapa). Libraries were denatured, flow cells set up using the cBot (Illumina), and run on a HiSeq 2500 using paired end 100 cycle protocols. For the AML tumor samples, 5 or 6 lanes were run per capture group. For the matched skin biopsy samples, 3 lanes (or equivalent) were run per capture group. The instrument and chemistry for all capture groups are provided in the Supplementary dashboard tables (Supplementary Information, Table S12,13).

For validation of sequencing results, an 11.9 megabase custom capture library was developed that provided coverage of all variants previously reported in AML as well as all new variants detected from exome sequencing in this study (Genes, Variants, and Capture Regions for this custom library are found in Supplementary Information, Table S14). This capture library was then applied to sequence 96 specimens that had previously been subjected to whole exome sequencing for validation of variant calls.

### Whole Exome Sequencing Data Processing

We developed customized analytical pipelines that combined published algorithms with novel filtering, curation, and quality control steps. Detailed depictions of analytical workflows are found in Supplementary Information (Table S6) and on our online browser ([http://vizome.org/additional\\_figures\\_BeatAML.html](http://vizome.org/additional_figures_BeatAML.html)). Initial data processing and

alignments were performed with commonly used analytical tools. For each flowcell and each sample, the FASTQ files were aggregated into single files for read 1 and 2. During this process these reads were trimmed by 3 on the 5' end and 5 on the 3' end. BWA MEM version 0.7.10-r789<sup>41</sup> was used to align the read pairs for each sample-lane FASTQ file. As part of this process, the flowcell and lane information was kept as part of the read group of the resulting SAM file. The Genome Analysis Toolkit (v3.3) and the bundled Picard (v1.120.1579) were used<sup>42</sup> for alignment post-processing. The files contained within the Broad's bundle 2.8 were used including their version of the build 37 human genome (These files were downloaded from: <ftp://ftp.broadinstitute.org/bundle/2.8/b37/>). The following steps were performed per sample-lane SAM file generated for each CaptureGroup:

- The SAM files were sorted and converted to BAM via SortSam
- MarkDuplicates was run, marking both lane level standard and optical duplicates
- The reads were realigned around indels from the reads--RealignerTargetCreator/IndelRealigner.
- Base Quality Score Recalibration

The resulting BAM files were then aggregated by sample and an additional round of MarkDuplicates was carried out at the sample level. Quality control reports were generated using the ReportingTools<sup>43</sup> and qrc<sup>44</sup> Bioconductor R packages along with sequencing core and alignment output files. Each AML sample BAM was paired with its skin biopsy pair and an additional round of indel realignment was carried out to ensure consistency of genotypes between the two samples. If an AML sample did not have a pair, the indel realignment was instead done at the sample level.

### Whole Exome Sequencing Variant Detection

For genotyping, each AML/skin biopsy pair was realigned at the sample level and then genotyped for single nucleotide variations using Mutect v1.1.7<sup>45</sup> and VarScan2 v2.4.1<sup>46</sup>. Indels were produced using VarScan2. Each variant call format (VCF) file was annotated using the Variant Effect Predictor v83 against GRCh37<sup>47</sup>. The resulting VCF files were filtered to include only those annotated to a gene and were converted to mutation annotation format (MAF) format using the vcf2maf v1.6.6 tool<sup>48</sup>.

Mutect v1.1.7<sup>45</sup> was run using default parameters except that no limit was placed on the number or frequency of the alternative allele frequency in the normal to help address normal contamination.

VarScan2 v2.4.1<sup>46</sup> was run in somatic mode with the recommended filtering scheme<sup>49</sup> except as shown in Supplementary Information, Table S23.

Indels and single nucleotide variants (SNVs) were produced for the tumor-only samples again using Mutect without a specified normal for consistency and VarScan2 in mpileup2indel or mpileup2snp mode respectively.



These variants were assigned to their most deleterious effect on Ensembl transcripts using Ensembl VEP v83 on GRCh37. This assignment was done using the same VEP parameters as the vcf2maf (v1.5.0) program.

The TCGA AML variants<sup>6</sup> in MAF form were downloaded from the GDC archive site: <https://portal.gdc.cancer.gov/legacy-archive/files/c410d927-d49c-4d4f-8356-601bee563ebe>. The MAF was converted to VCF files using the vcf2maf suite<sup>50</sup>. The resulting VCF files were lifted over from NCBI36 to GRCh37 of the human genome using CrossMap<sup>51</sup>. Only those variants that successfully lifted over were kept. Variants from Table S2 in Jaiswal et al 2014<sup>14</sup> were extracted and further processed removing variants that were ambiguous in terms of external sources and could not be found in their whole exome sequencing (WES) variants. The unique set of BeatAML variants was annotated relative to RefSeq transcripts using Ensembl VEP similar to above and all consequences were kept. This set of variants and consequences was searched against the set of processed Jaiswal variants.

Using the runs from MuTect and VarScan, these data were next filtered to keep only the protein impacting SNVs and indels from Mutect and VarScan2 and filtered requiring that the variants had at least 5 reads and either not be seen in the exome aggregation consortium (ExAC)<sup>52</sup> or be seen at a frequency < .01. These data present several additional challenges. First somatic calls cannot be obtained directly from the tumor-only samples, second there is always a possibility of tumor contamination of the skin samples for those samples that were paired. To address these issues and maximize comparability we used an iterative approach. The following was done separately for the two genotypers:

- An initial set of higher confidence somatic mutations were retrieved from the paired tumor/normal samples requiring tumor variant allele frequency (VAF)  $\geq 8\%$  and normal VAF  $\leq 5\%$  in addition to the significance tests already performed by the programs.
- A list of all candidate mutations was collated requiring that a mutation was either seen in the high confidence somatic set, the set of variants from Jaiswal et al or from the lifted over set of variants from the TCGA AML paper.
- Mutations from the overall set were kept if:
  - The overall number of calls in the paired samples was not more than twice the number of high confidence somatic calls
  - The tumor-only frequency for the calls was less than 50% greater than the number of calls in the paired samples
  - The mutation was seen in Jaiswal/TCGA list
- High Confidence somatic mutations were kept regardless

The data from the two genotypers were combined along with FLT3-ITD calls from Pindel<sup>53</sup>. Comparing our variant lists from whole exome sequencing versus our custom capture validation sequencing, we noticed, similar to others<sup>54</sup>, that low allele frequency C->A variants (< 15%) tended to have poor concordance (7.7%; data not shown) between the initial run and the technical validation run. These variants were removed in these data and

along with a curated 'blacklist' (Supplementary Information, Table S15) of known problematic variants/genes including mitochondrial DNA variants. In addition, all variants that were seen in a cumulative list of BeatAML normal samples at a frequency greater than 1% were removed. Cumulatively, of this set, 94% of covered single-nucleotide variants were validated with 82% of insertion/deletion calls also being confirmed with validation sequencing.

Manual review was then carried out in the following steps:

- a.) The addition back of all Jaiswal flagged rows.
- b.) Reviewed all TCGA flagged rows for VAF pattern that matched or did not match with known drivers in same specimen. Some TCGA variants were added back based on convincing VAF pattern and known pathogenic role, other TCGA variants were kept excluded based on VAF pattern unlike known drivers in same specimens.
- c.) Other variants were added back based on other specimens that had the same variant that was still on the include list and VAF pattern looked convincing for inclusion.
- d.) All Jaiswal genes with only frameshift/nonsense variants were manually reviewed and missense mutations were manually removed.
- e.) Genes/variants that were on both the include and exclude lists were manually reviewed and were removed if c to a with over 15% VAF, did not validate, and/or VAF pattern unlike known drivers in same specimen
- f.) Further review of all genes in summary sheet with cohort frequency of 8 or more (1% of more). Any that were not familiar from knowledge of AML literature were manually reviewed for VAF patterns that did or did not match known drivers within same specimens. Those that did not match were manually removed.

After this manual review, additional curated mutations from the UnifiedGenotyper run were added back in along with a curated set of variants from tumor-only patients in Jaiswal et al genes. The tumor-only AML samples utilized in Zhang et al (submitted) were removed and utilized for that study.

### Internal FLT3-ITD and NPM1 mutation detection

A subset of samples was tested for FLT3-ITD and NPM1 mutation status using an internally run PCR assay and capillary electrophoresis. Genomic DNA was extracted from fresh blood or bone marrow aspirates of AML patients was used to detect the presence or absence of FLT3-ITD and NPM1 4 bp insertion mutations<sup>55,56</sup>. Primers for FLT3 spanned approximately 330 bp to include the common internal duplication site<sup>55</sup>. Primers for NPM1 spanned approximately 170 bp to cover the clustered multiple insertional or insertion/deletion sites<sup>56,57</sup>. Primers were HPLC-purified by the manufacturer. The multiplex PCR reaction solution consisted of 100 ng gDNA, 10 pmol of the respective forward and reverse primers for FLT3 and NPM1, 25 mmol/l MgCl<sub>2</sub>, 2.5 mmol/l dNTP, 5 µl 10 × PCR buffer, 0.2

µl AccuTaq DNA polymerase and water in a total volume of 50µl<sup>58</sup>. The PCR conditions were: initial denaturing for 5 min at 94°C, followed by 30 cycles at 94°C for 30 s, 56°C for 45 s and 72°C for 30 s with a final cycle of 10 min at 72°C. The PCR products were diluted 1:10 and analyzed by capillary electrophoresis on a QIAxcel high resolution DNA cartridge according to the manufacturer's protocol.

Forward Primer *FLT3*: 5' - AGCA ATT TAG GTA TGA AAG CCA GCTA - 3'

Reverse Primer *FLT3*: 5' - CTT TCA GCA TTT TGA CGG CAA CC - 3'

Forward Primer *NPM1*: 5' - GTT TCT TTT TTT TTT TTT CCA GGC TAT TCA AG - 3'

Reverse Primer *NPM1*: 5' - CAC GGT AGG GAA AGT TCT CAC TCT GC - 3'

### Derivation of FLT3-ITD and NPM1 consensus calls

Consensus FLT3-ITD and NPM1 mutation calls found in the clinical summary table (Supplementary Information, Table S5) were determined by comparing the internal capillary PCR test (internal; method described above), the Clinical Laboratory Improvement Amendments/College of American Pathology (CLIA/CAP) laboratory run test (Sequenome, GeneTrails, Foundation Medicine, Genoptix, Illumina). The internal test was used for the sample consensus call when available as it was performed on the exact sample that was used for further *ex vivo* drug sensitivity assays. Where discordance existed between the internal test versus the CLIA lab test results, the sample was flagged for manual review. The trace file for the internal test was visually inspected and if discordance with the CLIA/CAP test results persisted, the whole exome sequencing data was then used to help determine the consensus call.

### Derivation of CCAAT enhancer binding protein alpha (CEBPA) biallelic consensus calls

N-terminal and C-terminal mutations have been described to occur on opposing alleles and patients harboring CEBPA biallelic mutations have been shown to fall into a favorable risk category<sup>59</sup>. Patients were scored positive for biallelic CEBPA mutation if described in the clinical notes as biallelic or double positive. Patients were also scored as CEBPA biallelic if both N-terminal and C-terminal mutations were identified in the whole exome sequencing data.

### RNA-Sequencing and Data Processing

All samples were sequenced using the Agilent SureSelect Strand-Specific RNA Library Preparation Kit on the Bravo robot (Agilent). Briefly, poly(A)+ RNA was chemically fragmented. Double stranded cDNAs were synthesized using random hexamer priming with 3' ends of the cDNA adenylated then indexed adaptors were ligated. Library amplification was performed using three-primer PCR using a uracil DNA glycosylase addition for strandedness. Libraries were validated with the Bioanalyzer (Agilent) and combined to run 4 samples per lane, with a targeted yield of 200 million clusters. Combined libraries were denatured, clustered with the cBot (Illumina), and sequenced on the HiSeq 2500 using a

100-cycle paired end protocol. In addition to the AML samples, there was also a sample of purified CD34 molecule (CD34)+ cells from healthy control bone marrow, which was included in each sample group (for a total of 12 times sequencing this control RNA). This control served as both a healthy comparator and a quality check on inter-group batch effects. 21 additional, individual healthy bone marrow samples were also included, two of which were CD34-selected (17-00053 and 17-00056) with the other 19 being whole mononuclear bone marrow cells from healthy donors.

Workflows for processing and analysis of RNA sequencing data to generate gene counts and gene fusions for each sample are shown on our online browser ([http://vizome.org/additional\\_figures\\_BeatAML.html](http://vizome.org/additional_figures_BeatAML.html)) with processed gene expression values for each specimen listed in Supplementary Information (Table S8,9). For each flowcell and each sample, the FASTQ files were aggregated into single files for read 1 and read 2 (if not already done by the sequencing core). During this process these reads were trimmed by 3 on the 5' end and 5 on the 3' end. Alignments of reads was performed using the subjunc aligner (1.5.0-p2)<sup>60</sup>. BAM files obtained from subjunc were used as inputs into featureCounts (1.5.0-p2)<sup>61</sup> and gene-level read counts were produced. For a reference genome, the GRCh37 build provided by the Broad as part of the GATK bundle was used. Gene assignments were based on the Ensembl build 75 gene models on GRCh37. See the parameters below for software usage.

```
subjunc -i /path/to/reference/ -u -r fastq1 -R fastq2 -o outputBAMFilename -I 5 -T 7 -d 50 -D 600 -S fr
```

```
featureCounts -a Homo_sapiens.GRCh37.75.gtf -o output -F GTF -t exon -g gene_id -s 2 -C -T 10 -p -P -d 50 -D 600 -B BAM_files
```

The data was collated from featureCounts matrices and all genes with no counts across the samples were excluded. Genes with duplicate gene symbols and those where the counts were < 10 for 90% or more of the samples were additionally removed prior to normalization similar to the approach suggested for weighted gene correlation network analysis (WGNCA)<sup>62</sup>. Samples for which their median expression was less than 2 standard deviations below the average were removed from the dataset (N=10). Normalization was performed using the conditional quantile normalization procedure<sup>63</sup>, which produced GC-content corrected log<sub>2</sub> reads per kilobase per million mapped reads (RPKM) values. This procedure produces both offsets to be used in conjunction with edgeR as well as a matrix of log<sub>2</sub> normalized RPKM values for clustering.

In addition, the subjunc BAM files were processed using the RNA-sequencing genotyping protocol (as of GATK v3.3) which was similar to the WES protocol described in the 'Whole Exome Sequencing' section including for each sample:

- MarkDuplicates
- SplitNCigarReads
- RealignerTargetCreator/IndelRealigner.
- Base Quality Score Recalibration

The resulting BAM files were used to produce RNA genotypes using the UnifiedGenotyper for the purposes of QC and ethnicity estimation.

Gene fusion data was additionally generated using the TopHat-Fusion (v2.0.14) program using default parameters<sup>64</sup>.

### Coexpression network formation

We formed coexpression modules using the WGCNA procedure on the RNA-sequencing data from the 'RNA-Sequencing and Data Processing' section. All RNA-sequencing samples were used to form the set of modules. Due to the heterogeneity of clinical expression data we generated 'signed hybrid' networks using 'bicor' correlation setting the max proportion of outliers to .1<sup>65</sup>. We ran the procedure multiple times, varying several parameters to choose the most relevant set for further analysis. The WGCNA procedure was run on datasets formed from the top 2,000 and 5,000 most variable genes. For each dataset we set the 'power' variable to either 2 or 3. For each of these runs we varied the module detection parameters of dynamicTreeCut<sup>62</sup>, namely the deepSplit parameter was set to 0 or 2 and the pamStage parameter was set to TRUE or FALSE. For each of these sets of modules we computed a series of module quality statistics<sup>66</sup>, mean correlation, mean adjacency, mean MAR, mean KME, proportion of variability explained and the mean cluster coefficient. Significance of modules was determined by computing a Zscore of each of these values relative to the mean and standard deviation of those from 100 random assignment of modules. We chose the set of modules to use in our analyses as those that were most correlated with the 'specimenSpecificDx' using the module quality as a tie-breaker. The analysis set of modules was chosen to be the version using the 5,000 most variable genes, power set to 2 and modules formed using deepSplit=2 and pamStage=F. Of this set of modules only the grey module didn't have a summary Z statistic (median across the 4 density measures) of at least 2. Additionally after correcting the data using the estimated principal components<sup>67</sup>, the module structure didn't change appreciably (data not shown).

### Quality Control

The UnifiedGenotyper runs for both the WES and RNA-sequencing were combined into a single VCF file using the GATK CombineVCFs functionality. This combined VCF file was converted to a GDS file using SNPRelate (1.12.2)<sup>68</sup>. Note the version is an upper bound as several versions were used across the entire project). The overall similarity of the genotypes of each pair of samples were computed, termed identity by state (IBS) and a hierarchical clustering was performed using one minus this similarity. From this clustering and visualization we had devised hard cutoffs for further inspection based on the types of data being compared. For instance samples not meeting the specified IBS thresholds (DNA-DNA=.9; RNA-RNA=.83; DNA-RNA=.89) were subject to manual review. Based on the dendrogram structure as well as the clinical/lab information, samples were either excluded, assigned to a different patient ID or in rare cases assigned to a different sample. It was observed that bone marrow transplants between sample collections produced a noticeable but milder effect in these dendrograms and such samples were flagged for removal in RNA-sequencing analysis and for treatment as tumor-only samples in the WES analysis as is described in the 'WES Variant Detection' section.

### Fusion annotation for analysis

Fusions calls were determined from a consensus of three datatypes, a specific diagnosis categorization at the time of sample acquisition, current set of clinical karyotypes and fusions detected in RNA-sequencing data by TopHat-Fusion. All sources were limited to the same set of known fusions: RUNX1-RUNX1T1, CFBF-MYH11, MLLT3-KMT2A, DEK-NUP214, GATA2-MECOM and PML-RARA. It was determined that the RNA-sequencing calls did not provide additional resolution in detecting these known fusions and was not performed on all the samples so the consensus was limited to the clinical karyotype calls as well as the specific diagnosis categorization (which was determined based on karyotype and other cytogenetic clinical tests). Overall the calls were based on the karyotype data except in 10 cases, 3 where the karyotype and diagnosis was sufficiently complex to warrant a separate 'Complex' categorization. The remaining 7 of these cases were set to the specific diagnosis classification. It should be noted there was additional support from the RNA-sequencing data for several of these cases.

### Ethnicity

The combined RNA and WES VCF from the 'Quality Control' step was merged with a set of Hapmap genotypes<sup>69</sup> lifted over to build 37. The SNPRelate package was used to convert the VCF to GDS, perform LD pruning using an LD threshold of .2, MAF cutoff of .05 and allowing a missing rate of .3 and calculation of the principal components. The methodology of Zheng and Weir 2015<sup>70</sup> was used to assign admixture proportions relative to the HapMap samples using the principal components. Each sample was assigned to an ethnicity group based on the group with the maximum admixture proportion. If the maximum was 50% or less, we labeled it *Admixed*. As we have observed previously that the clustering of ethnicities for RNA-sequencing samples are more diffuse than exome sequencing, we assigned the final inferred ethnicity to each patient based on the distinct WES calls if available, deferring to RNA-sequencing only if not available. If multiple exome sequencing samples were present with discrepant calls, the patient was subject to manual review. The only patient where this occurred was patient 4043, a self-identified Hispanic who had 2 RNA samples and an exome sequencing sample inferred as White and one exome sample inferred to be HispNative. Only the White call for the exome sequencing had an admixture proportion over .5. The patient was kept consistent with the self-identification and labeled as HispNative.

### Sex

For DNA, coverage is first computed over the Y chromosome and the counts for each sample are added up and log10 transformed (after adding 1 to all the counts). K-means clustering is used to assign samples to 2 clusters with the cluster with the lower mean labeled as the Female cluster.

For RNA-sequencing, counts were converted to counts per million (CPM) after applying the Trimmed Mean of M scaling normalization<sup>71</sup>. A set of 28 genes chosen to successfully discriminate the genders via DE analysis over multiple studies (data not shown) were used in conjunction with Kmeans clustering to form two clusters. The *Female* cluster was labeled based on high *XIST* expression.



## ELN 2017 Classification

This procedure is based off of the categorization in Table 5 of the 2017 ELN update paper<sup>5</sup>

Karyotypes in the clinical file were first cleaned and parsed into clones/subclones and distinct abnormalities using standard conventions<sup>72</sup>. The current representation was corrected for nomenclature type (e.g. *idem* vs *sl*) in a basic manner. For instance, ambiguous events such as chromosomal loss (e.g. -15) was not corrected for whether the preceding clone had a counteracting gain. Also, additional +/- symbols in conjunction with valid karyotype operators in a separate clone (e.g. +del(12)(q?15) or -del(12)(q?15)) were treated separately with gains (+) being kept in the unique count of events and losses (-) being removed.

Abnormalities were first checked for the following categories:

1. **RUNX1-RUNX1T1**
2. **CBFB-MYH11**
3. **MLLT3-KMT2A**
4. **DEK-NUP214**
5. **KMT2A-\***
6. **BCR-ABL1**
7. **GATA2-MECOM**
8. -5/del(5q) (termed minus\_5)
9. -7 (termed minus\_7)
10. -17 (termed minus\_17)

Note the bold were further considered to be WHO recurrent fusions.

The number of unique abnormalities (across clones) was then computed.

Whether or not a karyotype was considered to be polyploid was also recorded (at least 60 chrs or '(>=3)n' or label).

NPM1, FLT3-ITD, and biallelic CEBPA were derived from consensus calls. FLT3-ITD allelic ratios were determined solely for the samples with an internal assay. The MAF values of the internal assay were converted to a ratio using the formula  $MAF/(1-MAF)$ .

RUNX1, ASXL1 and TP53 were derived from the clinical genotypes.

Abn\_17 calls were manually curated from the karyotype data and clinical genotype calls respectively.

The determination of ELN 2017 categories proceeds by assigning TRUE/FALSE/NA values to one or more of the 5 columns (3 ELN and 2 ambiguous) in the following way:

1. isFavorable is considered TRUE if a sample has at least one of the following:

- a. RUNX1-RUNX1T1
  - b. CFBF-MYH11
  - c. Positive NPM1 and negative FLT3-ITD
  - d. Positive NPM1 and positive FLT3-ITD with allelic ratio  $< .5$
  - e. Biallelic CEBPA
2. isFavorableOrIntermediate
- a. NPM1 is positive and FLT3-ITD is positive but the allelic ratio is not available
3. isAdverse is considered TRUE if a sample has at least one of the following:
- a. DEK-NUP214
  - b. KMT2A-\*
  - c. BCR-ABL1
  - d. GATA2-MECOM
  - e. minus\_5
  - f. minus\_7
  - g. minus\_17
  - h. abn\_17
  - i. 3 or more abnormalities and not a WHO recurrent fusion
  - j. One monosomy (autosomal) and at least one additional abnormality except for CFBF-MYH11
  - k. Positive RUNX1 or ASXL1 and not considered to be isFavorable or isFavorableOrIntermediate
  - l. Positive TP53
4. isIntermediate is considered TRUE if a sample has at least one of the following:
- a. MLLT3-KMT2A
  - b. NPM1 positive and positive FLT3-ITD with allelic ratio  $\geq .5$
  - c. NPM1 negative and negative or low allelic ratio ( $<.5$ ) FLT3-ITD
  - d. At least one abnormality and is not considered isFavorable or isAdverse
5. isIntermediateOrAdverse
- a. NPM1 negative and FLT3-ITD positive without an allelic ratio

NAs occur in the absence of FLT3-ITD or NPM1 calls.

Samples where the specific diagnosis at inclusion indicated 'Acute promyelocytic leukaemia with t(15;17)(q22;q12)' were automatically set to 'Favorable'.

Any overlaps of the categories were resolved based on manual expert review.

### **Ex vivo Functional Drug Screens**

Ex vivo functional drug screens were performed on freshly isolated mononuclear cells from AML samples. Briefly, 10,000 cells per well were arrayed into three, 384-well plates containing 122 small-molecule inhibitors. This panel contained graded concentrations of a drugs with activity against two-thirds of the tyrosine kinome as well as other non-tyrosine kinase pathways, including mitogen activated protein kinases (MAPKs), phosphatidylinositol-4,5-bisphosphate 3-kinase/AKT serine/threonine kinase 1/mechanistic target of rapamycin kinase (PIK3C/AKT/MTOR), protein kinase AMP-activated (AMPK/PRKAA), ATM serine/threonine kinase (ATM), Aurora kinases, calcium/calmodulin dependent protein kinases (CAMKs), cyclin-dependent kinases (CDKs), serine/threonine protein kinase 3 (GSK3), I-kappaB kinase (IKK), cAMP dependent protein kinase (PKA), protein kinase C (PKC), polo-like kinase 1 (PLK1), and RAF proto-oncogene serine/threonine kinase (RAF). In addition, the library contained small molecule inhibitors with activity against the BCL2 family, bromodomain containing 4 (BRD4), Hedgehog, heat shock protein 90 (HSP90), NOTCH/gamma-secretase, proteasome, survivin, signal transducer and activator of transcription 3 (STAT3), histone deacetylase (HDAC), and WNT/beta-catenin. Drug plates were created using inhibitors purchased from LC Laboratories and Selleck Chemicals and master stocks were reconstituted in dimethyl sulfoxide (DMSO) and stored at  $-80^{\circ}\text{C}$ . Master plates were created by distributing a single agent per well in a seven-point concentration series, created from three-fold dilutions of the most concentrated stock resulting in a range of  $10\ \mu\text{M}$  to  $0.0137\ \mu\text{M}$  for each drug (except dasatinib, ponatinib, sunitinib, and YM-155 which were plated at a concentration range of  $1\ \mu\text{M}$  to  $0.00137\ \mu\text{M}$ ). DMSO control wells and positive control wells containing a drug combination of Flavopiridol, Staurosporine and Velcade were placed on each plate, with the final concentration of DMSO  $\leq 0.1\%$  in all wells. Daughter plates were created using a V&P Scientific 384-well pin tool head operated by the Caliper Sciclone ALH 3000 and equipped with 0.457mm diameter, 30 nanoliter, slotted stainless steel pins (cat num: FPINS30). Daughter and destination plates were sealed with peelable thermal seals using a PlateLoc thermal sealer. Destination plates were stored at  $-20^{\circ}\text{C}$  for no more than three months and thawed immediately before use. Primary mononuclear cells were plated across single-agent inhibitor panels within 24 h of collection. Cells were seeded into 384-well assay plates at 10,000 cells per well in Roswell Park Memorial Institute (RPMI) 1640 media supplemented with fetal bovine serum (FBS) (10%), l-glutamine, penicillin/streptomycin, and  $\beta$ -mercaptoethanol ( $10\text{--}4\ \text{M}$ ). After 3 d of culture at  $37^{\circ}\text{C}$  in 5%  $\text{CO}_2$ , MTS reagent (CellTiter96 AQueous One; Promega) was added, optical density was measured at 490 nm, and raw absorbance values were adjusted to a reference blank value and then used to determine cell viability (normalized to untreated control wells).

### **Ex vivo Functional Drug Screen Data Processing**

A workflow summarizing data normalization, curve fit parameters, and quality assurance/quality control (QA/QC) steps is found on our online browser ([http://vizome.org/additional\\_figures\\_BeatAML.html](http://vizome.org/additional_figures_BeatAML.html)) with processed drug response data for each specimen listed in Supplementary Information (Table S10). A given sample was run on one or more

panels and within each panel, the majority of drugs were run without within-panel replicates. Two steps were performed to harmonize these data prior to model fitting:

1. A ‘curve-free’ AUC (integration based on fine linear interpolation between the 7 data points themselves) was calculated for those runs with within-panel replicates after applying a ceiling of 100 and a floor of 0 for the normalized viability. The maximum change in AUC amongst the replicates was noted and those runs with differences > 100 were removed.
2. Remaining within-plate replicates had their normalized viability averaged and subject to a ceiling of 100 and floor of 0. An additional set of ‘curve-free’ AUCs was computed for sample-inhibitor pairs run on multiple panels. The maximum change in AUC amongst the across-panel replicates was noted and those runs with differences > 75 were removed.

At this point, the within and across plate replicates for the normalized viability were averaged together and a ceiling of 100 was applied. From the steps above, the floor was already at 0.

Based on the methodology used in our prior drug combination study<sup>73</sup>, a probit regression was fit to all possible run groups using the model:

$$(\text{normalized\_viability} / 100) \sim 1 + \log_{10}(\text{concentration})$$

Where for all groups there were N=7 dose-response measurements.

The summary measures of curve fit were inspected and cutoffs were devised removing all runs with an AIC > 12 and deviance > 2. For inhibitors that were run using multiple concentration ranges, only the latest concentration range was kept. Finally, these data were compared to the AUC values from third order polynomial fits. Those runs that were discrepant in terms of sensitive/resistant calls were manually reviewed as subject to removal.

### **Ex vivo Functional Drug Screen Analysis**

For all drug analyses requiring a call of sensitivity or resistance (e.g. the gene expression signatures), sensitivity/resistance was determined by the lowest and highest 20% of the AUC values for each drug.

**Correlations between drugs in families**—For each inhibitor in the study, available data on targets of the inhibitors were pulled from a variety of online resources and published studies, many of which were aggregated in the Cancer-Targetome<sup>74,75</sup>. Activity of each inhibitor for targets was then distilled into a 5-tier system to afford comparison across drugs with differing degrees of potency and/or for which differing assays were used to measure drug/target activity. Well-represented genes, gene families, and pathways were then filtered for drugs having activity in the top 3 tiers for one or more member of the gene family or pathway. These lists were then manually curated to arrive at a final list of high-confidence drug target families (shown in Supplementary Information, Table S11). For each inhibitor assigned to at least one drug target family, the Pearson’s correlation was computed against

all other drugs assigned to at least one drug target family for the AUC values of all available samples shared between the two drugs.

**Correlations between drugs/samples**—Drugs were first filtered requiring greater than two hundred samples per drug. Additional samples were removed accordingly to allow correlations to be computed between all present samples using available AUC data and between all drugs.

**Summary Drug Response Scores**—For each patient sample, a binary encoding (1/0) was used for each drug based on same threshold as for the gene signatures (e.g., sensitivity/resistance was determined by the lowest and highest 20% of the AUC values for each drug). Individual scores were computed for resistance and sensitivity separately and represented as the proportion over all drugs screened for each patient sample.

### Expression Analysis and Integration with *Ex Vivo* Functional Drug Screen

For all the below analyses the earliest sample was chosen for each patient.

**Expression heatmap**—The top 2,000 most variable genes were extracted. The expression values were centered and scaled across patients and complete-linkage hierarchical clustering was performed using the ComplexHeatmap R package<sup>76</sup>.

**Sensitive/Resistant differential expression**—For each drug, it was required that at least 3 sensitive and 3 resistant samples using the 20%/20% criteria outlined in the ‘Drug Analysis’ section. Patient samples were limited to those labeled as sensitive or resistant. Next, genes were limited based on their expression, where at least half the patients used for analysis had to have greater than one counts per million (an approach suggested in the limma users manual<sup>77</sup>. The normalized expression as in the ‘RNA-Seq Processing’ section data with the chosen samples and genes was used for differential expression analysis. As the data had not been batch corrected at this point, surrogate variable analysis (SVA)<sup>78</sup> was used to infer covariates for correcting out technical confounders. Next the linear model fitting for each gene was performed using the limma-trend approach<sup>79</sup> testing whether the average expression was different between resistant – sensitive correcting for the SVA covariates. Genes with Benjamini-Hochberg (BH)<sup>38</sup> FDR values of less than .05 were kept for the cluster analysis. The expression matrix was corrected with respect to the estimated surrogate variables for consistency with the differential expression procedure using fSVA<sup>80</sup> and Mclust<sup>81</sup> was used to determine optimal number of clusters and parameterization. The results were then visualized using a clusplot<sup>82</sup> which displays the clustering results with respect to the first two principal components of the gene expression for the kept genes.

### Mutation Analysis and Integration with *Ex vivo* Functional Drug Screen

For all the below analyses where groups of samples were compared, the earliest sample was chosen for each patient.

**TCGA comparison**—The lifted over TCGA variants from the ‘WES Variant Detection’ section were annotated using the VEP from Ensembl build 83, filtered for protein-altering

and splice site variants and our ‘blacklist’ was applied to ensure the variant sets were comparable.

**Co-occurrence/mutual exclusivity**—Only mutations seen in at least 10 patients were kept. The DISCOVER<sup>40</sup> method was used to determine significant mutual exclusivity and co-occurrence. A plot of the co-occurrences was generated using corrplot<sup>83</sup> with the odds ratio of the pairwise co-occurrence used to color and scale the circle sizes.

**Mutation/drug association**—For each mutated gene in the exome sequencing samples and each recurrent fusion (counting FLT3-ITD as a distinct entity from other FLT3 mutants) we determined all available (at least 5 patients) pairwise and three-way co-occurrence sets. For each drug and each valid set of genes (from one to three genes) we fit a linear model with AUC as the response and examined the linear contrast (i.e., two-sided t-test) comparing the AUC of the gene(s) to the appropriate negative. For example the average AUC of the FLT3:DNMT3A:NPM1 mutants would be compared to average AUC of the samples negative for all three genes. FDR was computed using the BH over all the drugs.

For the Ibrutinib and entospletinib comparisons, the presence and absence of the 3 genes/mutations: NPM1, FLT3\_ITD and DNMT3A was collapsed into levels of a single factor. The corresponding single factor ANOVA was carried out with the ‘triple negative’ category set as the reference. Significance of the p-values of each coefficient were compared to the Bonferroni corrected .05 level.

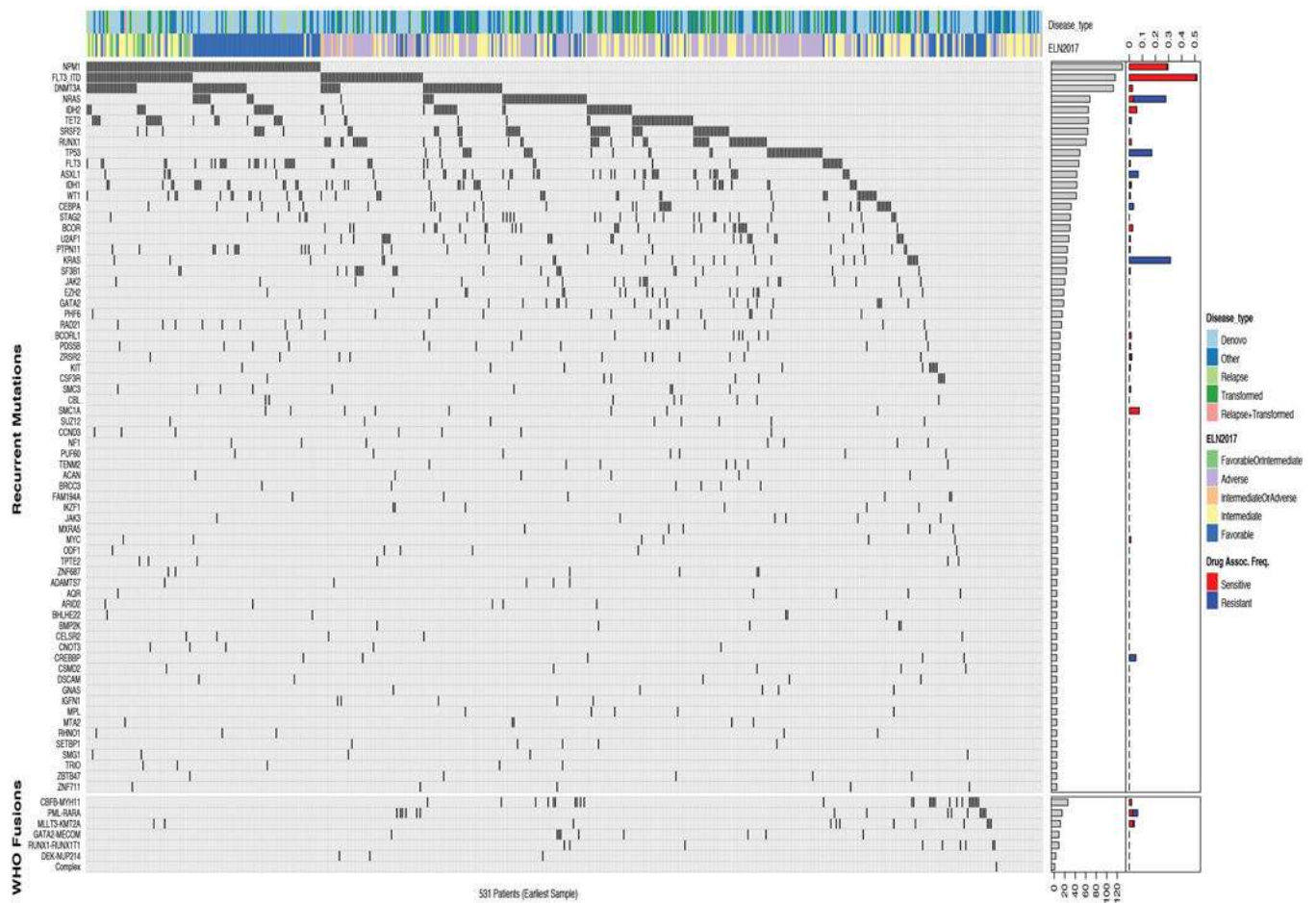
For the JAK-family analysis, the AUC values were pooled for the four JAK inhibitors (CYT387, Tofacitinib (CP-690550), JAK Inhibitor I, Ruxolitinib (INCB018424)) for each gene mutation set (BCOR, BCOR:DNMT3A, BCOR:RUNX1, BCOR:SRSF2). The contrast of the difference between BCOR:RUNX1 samples and the average of the other three mutation groups was tested.

### **Integration of both mutation and RNA-Sequencing with *Ex vivo* Functional Drug Screen**

Mutations (0/1 encoding) and the module eigengenes from the WGCNA analysis were used separately and combined together in regression models with coefficients selected using the lasso approach<sup>84</sup> as implemented in glmnet<sup>85</sup>. For each datatype and the combination, only drugs with at least 200 patients samples were tested. The 3 datasets were initially randomly separated into training (75%) and test (25%) sets. Similar to a previous approach<sup>86</sup>, a bootstrap aggregation approach was used where the 1,000 bootstraps of the training dataset was generated and for each one, the lasso trained using 10 fold cross-validation. Predictions were formed for the test dataset over these bootstrap models and the predicted AUC was averaged.  $R^2$  values were computed for these aggregated predictions relative to the test AUC values. As performance was seen to be dependent on the initial test/training split, we repeated the entire process 100 times, recording the mean and standard deviation of the  $R^2$  value as well as the count non-zero coefficients.



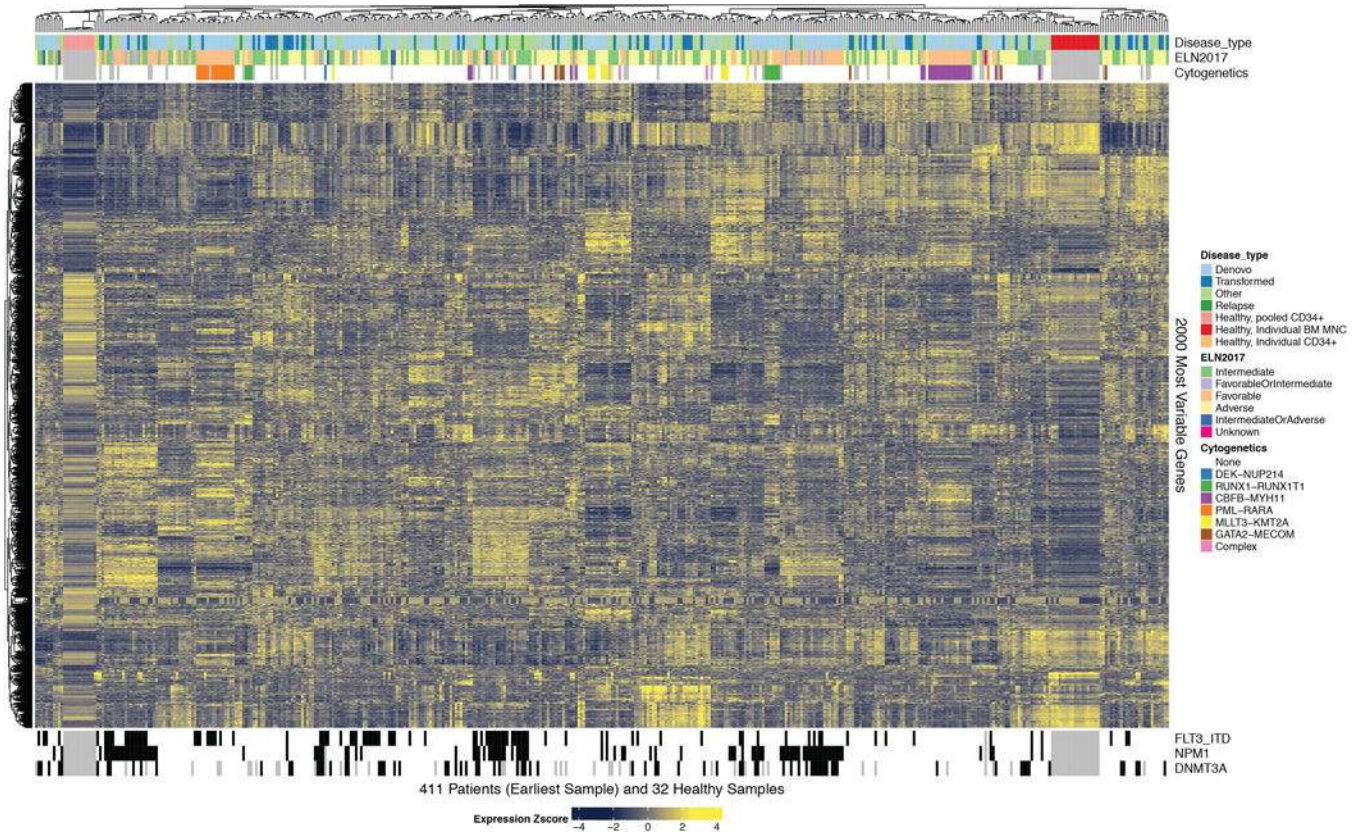
Extended Data



**Extended Data Fig. 1. Genomic Landscape of the Beat AML Cohort.**

622 specimens from 531 unique patients were subjected to whole exome sequencing. Automated and manual curation steps (described in the Methods, Supplementary Information, and at [http://vizome.org/additional\\_figures\\_BeatAML.html](http://vizome.org/additional_figures_BeatAML.html)) were used to arrive at a final set of high confidence variants (annotated in Supplementary Information, Table S7) and the earliest sample for each unique patient was used in this analysis. Clinical cytogenetics and gene fusion calls from RNA-sequencing were used to curate recurrent gene rearrangements (Supplementary Information). The mutational profile for each unique patient is shown with frequency ranked mutational events in the upper portion and frequency ranked gene rearrangements in the lower portion. The mosaic plot is annotated with clinical features of each case, such as diagnosis/relapse and *de novo*/transformed disease states and the first bar chart to the right summarizes the cohort frequencies of mutational and gene rearrangement events. The last bar chart on the right summarizes the frequency of significant drug/mutation associations for the given gene across the cohort with drug sensitivity displayed in red and drug resistance displayed in blue. Eleven genes not previously reported to be somatically mutated in cancer were observed with mutations at ~1% cohort frequency: CUB and Sushi multiple domains 2 (CSMD2), NAC alpha domain containing (NACAD), teneurin transmembrane protein 2 (TENM2), aggrecan (ACAN), ADAM metallopeptidase

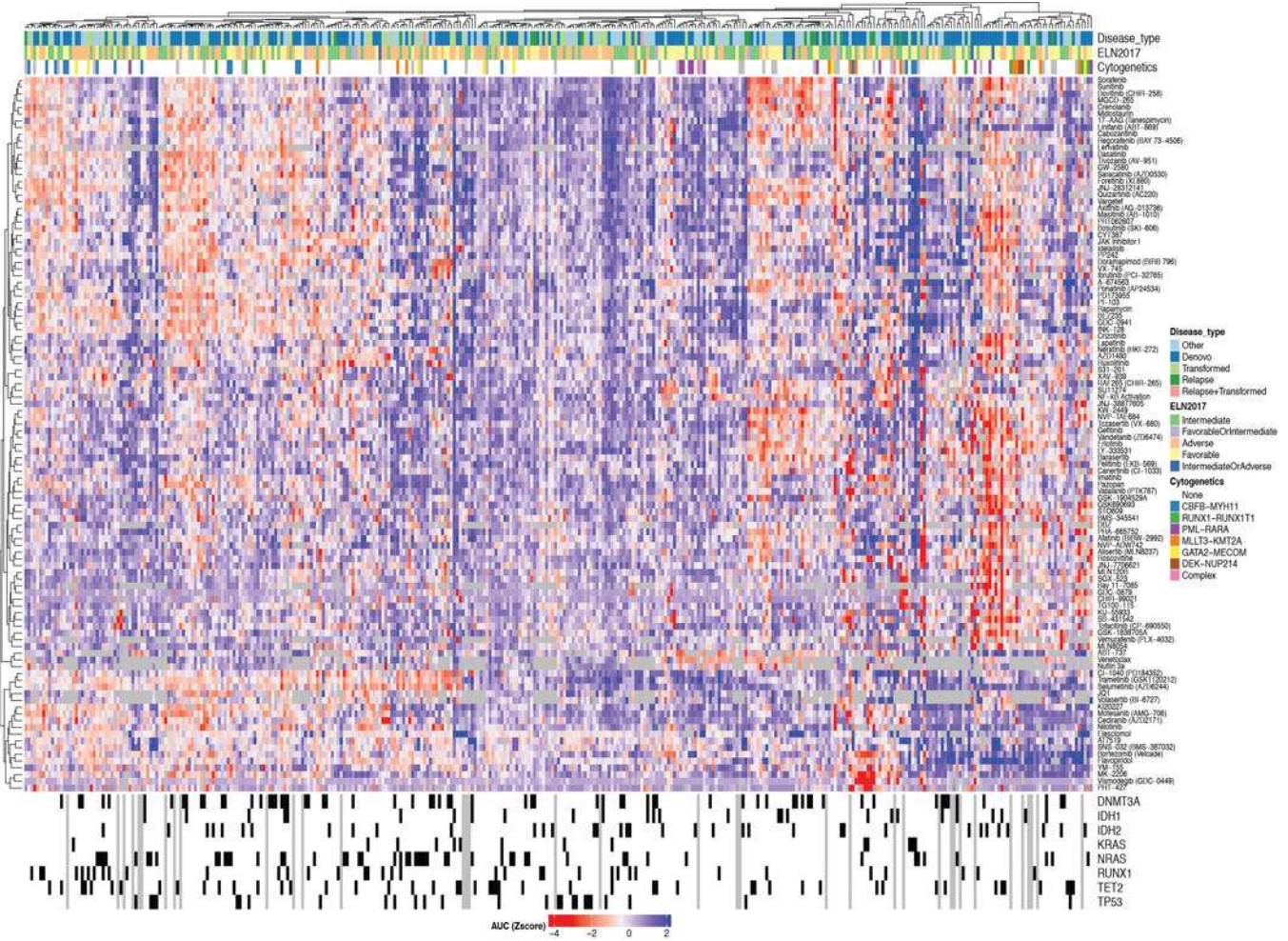
with thrombospondin type 1 motif 7 (ADAMTS7), immunoglobulin-like and fibronectin type III domain containing 1 (IGFN1), neurobeachin like 2 (NBEAL2), poly(U) binding splicing factor 60 (PUF60), zinc finger protein 687 (ZNF687), cadherin EGF LAG seven-pass G-type receptor 2 (CELSR2), and glutamate ionotropic receptor NMDA type subunit 2B (GRIN2B). For the  $n$  used to correlate each drug with mutations, please see Supplementary Information (Table S17).



**Extended Data Fig. 2. Transcriptomic Landscape of the Beat AML Cohort.**

451 specimens from 411 unique AML patients were subjected to RNA-sequencing. The 2,000 genes with greatest differential expression across these unique AML patients are displayed on the heatmap. The heatmap is annotated with disease type, ELN risk stratification groups, genetic, and cytogenetic features of disease as noted in the figure legend.





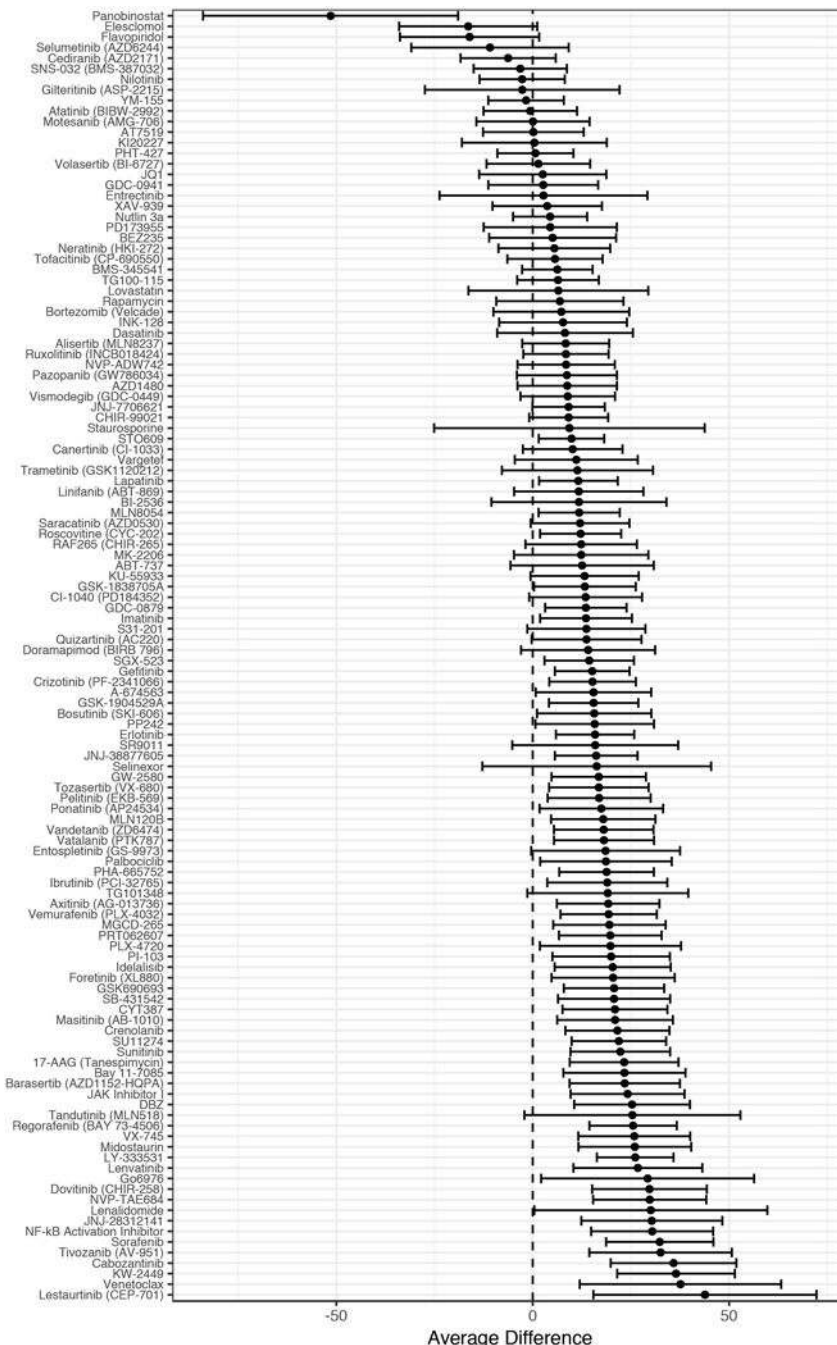
**Extended Data Fig. 3. Functional Drug Sensitivity Landscape of the Beat AML Cohort.** 409 specimens from 363 unique AML patients were subjected to an *ex vivo* drug sensitivity assay whereby freshly isolated mononuclear cells from blood or bone marrow of patient specimens were incubated with graded concentrations of 122 small-molecule inhibitors (7 dose points in addition to the no drug control). Probit curve fits were used to compute drug response metrics, and the z-score of area under the dose response curve is plotted for each unique patient specimen against each drug. Drug sensitivity (blue) and resistance (red) are annotated by a color gradient, with grey indicating no drug data available. The heatmap is annotated at the top and bottom with major clinical, cytogenetic, and genetic features of disease as noted in the figure legend.

Author Manuscript

Author Manuscript

Author Manuscript

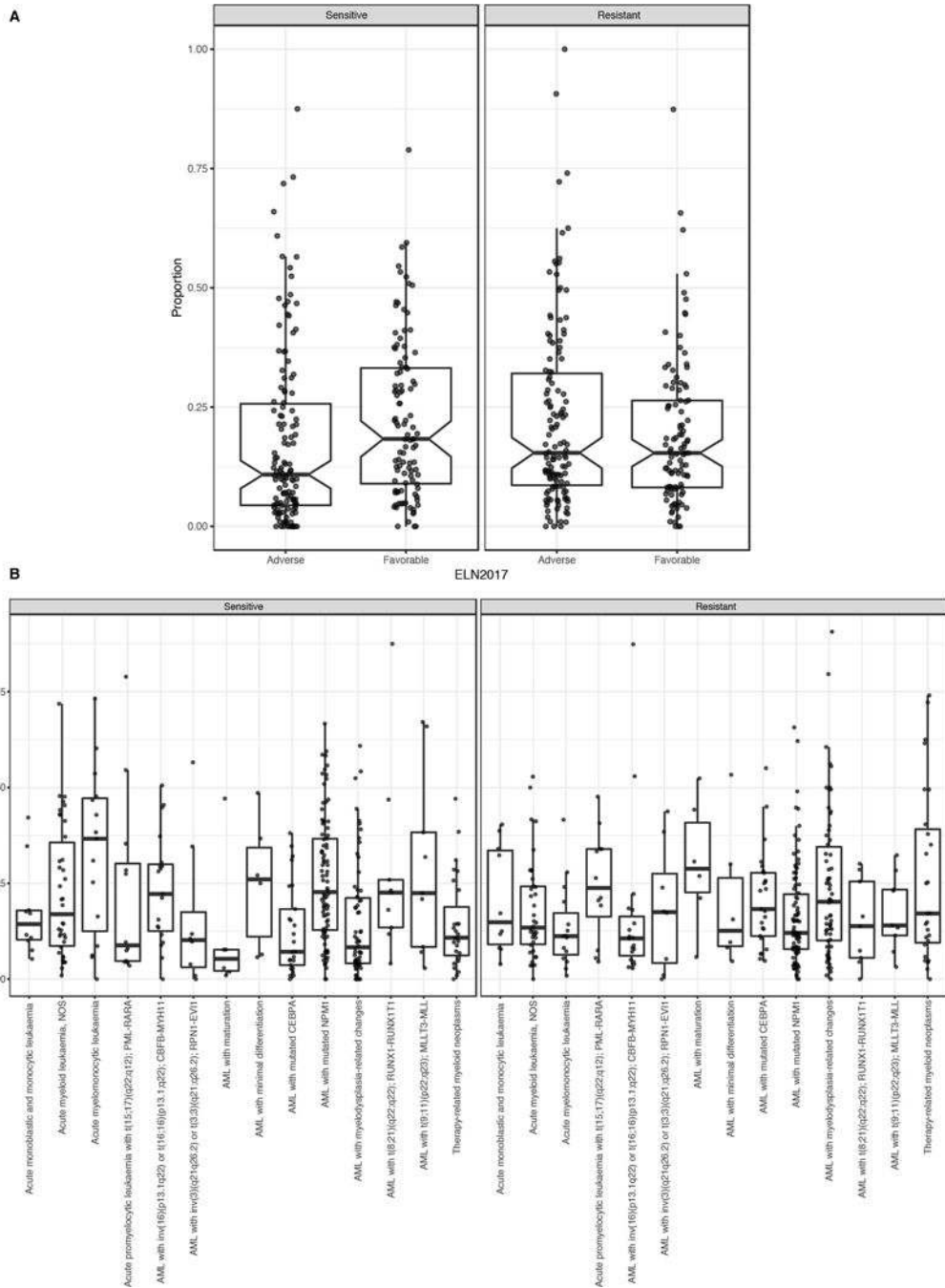
Author Manuscript



**Extended Data Fig. 4. Drug response in *de novo* versus transformed AML cases.**  
 The average inhibitor response AUCs for all cases that were *de novo* (n=288) versus all cases that transformed from a background of MDS (n=111) were compared for every inhibitor having at least 3 cases with evaluable data in each group. The middle point represents the average difference in AUC between the two groups with the bars representing the 95% confidence interval. For the sample size and statistical results of each drug/sample group correlation please see Supplementary Information (Table S20).





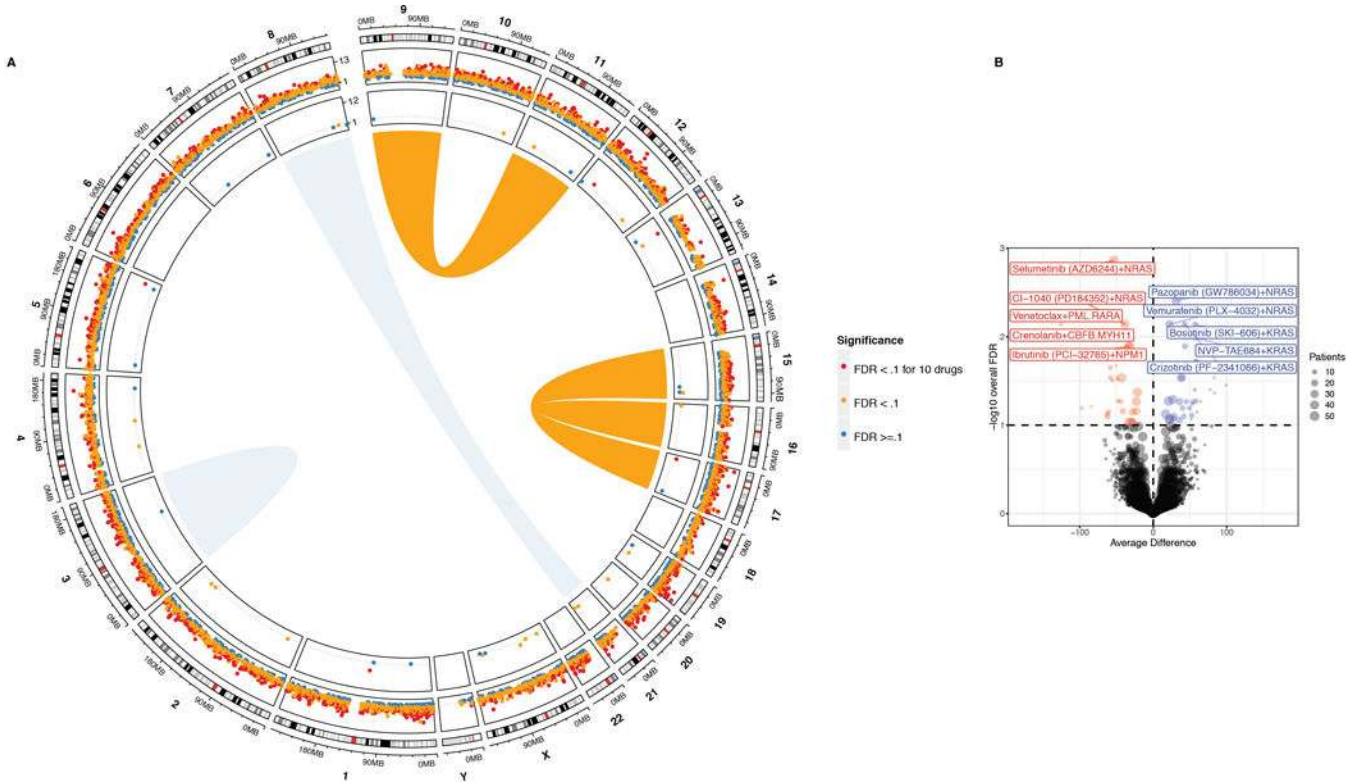


**Extended Data Fig. 6. Binary Drug Response Calls and Correlation with Clinical Subsets.**  
**A.** For the intersect of every specimen with evaluable response data for each inhibitor, we created a threshold for binary sensitive/resistant calls based on whether the individual specimen response fell within the most sensitive 20% of all specimens tested against that drug. A matrix plot showing the unsupervised clustering of the binary calls can be found at [http://vizome.org/additional\\_figures\\_BeatAML.html](http://vizome.org/additional_figures_BeatAML.html). The binary drug resistance calls for each specimen were rolled up into a single value representing the proportion of drugs to which an individual specimen was sensitive (left) or resistant (right). Specimens were



divided into Favorable and Adverse groups based on ELN 2017 criteria to determine whether overall drug sensitivity/resistance correlated with prognostic features of disease (n=233 patients).

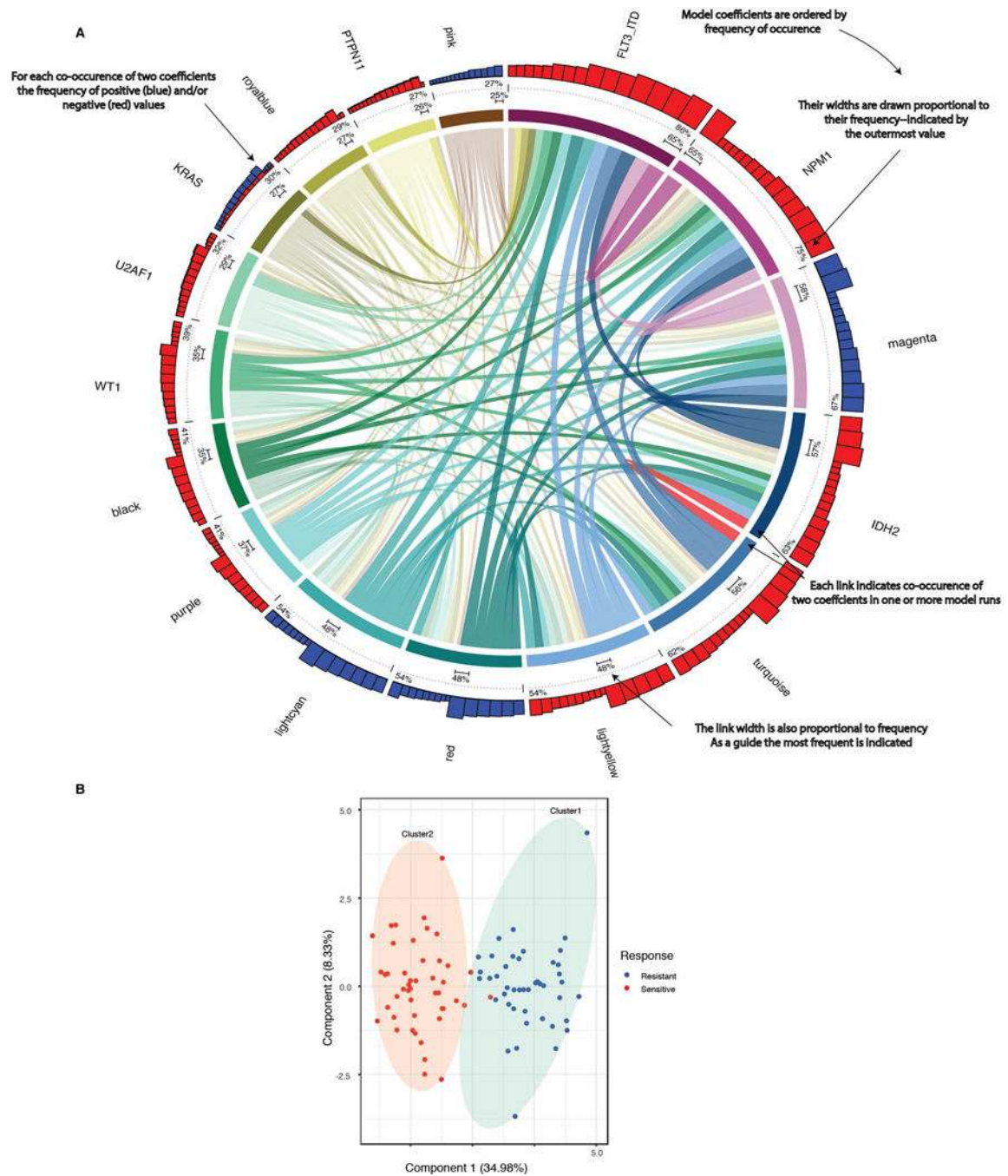
**B.** The binary drug resistance calls for each specimen as in panel B. Specimens were divided into diagnostic groups based on WHO 2016 categories to determine whether overall drug sensitivity/resistance correlated with cytogenetic or morphologic features of disease (n=340 patients). For both A and B the upper and lower points of the boxplots show 1.5 times the interquartile range (IQR) from the upper/lower lines while the upper, middle and bottom lines indicate the 75th, median and 25th percentile of the data with the notches extending  $1.58 * IQR / \sqrt{n}$ . Specific sample sizes of each group are reported in Supplementary Information (Table S22).



**Extended Data Fig. 7. Integration of Genetic Events with Drug Sensitivity.**

(A) Circos plot showing AML rearrangements in the center, mutational events in the next concentric ring, and gene expression events in the outer ring. The size/width indicates frequency of the event and FDR-corrected q-value of association with drug sensitivity is color-coded (sensitivity (red); resistance (blue)). For each gene, tests involving expression were two-sided t-tests (linear model) of the differences between sensitive and resistant samples. For mutational events, the average difference in AUC between mutant/wild type samples was determined using two-sided t-tests from a linear model as shown in Fig 2A. FDR was computed using the Benjamini-Hochberg over all the drugs. The n used to correlate each mutational event with drug sensitivity is reported in the Supplementary Information (Table S17).





**Extended Data Fig. 9. Functional Drug Sensitivity Landscape of the Beat AML Cohort.**  
**A.** Co-occurrences with regard to WGCNA gene expression clusters and/or mutational events (coefficients) were detected by multivariate modeling with respect to ibrutinib response (resistance (blue); sensitivity (red)) with degree of correlation quantified in top track stacked barplot. All coefficients that appear in 25% of the bootstrap sample sets are shown as segments of the circle. Segment width (the colored ring) corresponds to the percentage of bootstrap samples in which that coefficient appears (quantified above the dotted line). The variables appear in descending order clockwise starting at 12 o'clock. Each

link indicates pairwise co-occurrence of mutational events and gene expression clusters (width represents frequency of the co-occurrence). The largest co-occurrence for each coefficient is quantified.

**B.** The capacity of differential gene expression to distinguish the 20% most ibrutinib sensitive (n=46) from 20% most resistant (n=44) specimens is shown on a principle component plot (n=239 patient samples total tested for ibrutinib sensitivity and RNA-Sequencing).

For the n used to correlate each drug with gene expression and perform Lasso regression, please see Supplementary Information (Table S17).

## Supplementary Material

Refer to Web version on PubMed Central for supplementary material.

## Authors

Jeffrey W. Tyner<sup>1,2</sup>, Cristina E. Tognon<sup>2,3,4</sup>, Dan Bottomly<sup>2,5</sup>, Beth Wilmot<sup>2,5,6</sup>, Stephen E. Kurtz<sup>2,3</sup>, Samantha L. Savage<sup>1,2</sup>, Nicola Long<sup>2,3</sup>, Anna Reister Schultz<sup>1,2</sup>, Elie Traer<sup>2,3</sup>, Melissa Abel<sup>1,2</sup>, Anupriya Agarwal<sup>2,7</sup>, Aurora Blucher<sup>2,5</sup>, Uma Borate<sup>2,3</sup>, Jade Bryant<sup>1,2</sup>, Russell Burke<sup>2,3</sup>, Amy Carlos<sup>2,8</sup>, Richie Carpenter<sup>2,3</sup>, Joseph Carroll<sup>2,9</sup>, Bill Chang<sup>2,10</sup>, Cody Coblentz<sup>2,3</sup>, Amanda d'Almeida<sup>1,2</sup>, Rachel Cook<sup>2,3</sup>, Alexey Danilov<sup>2,3</sup>, Kim-Hien T. Dao<sup>2,3</sup>, Michie Degnin<sup>2,3</sup>, Deirdre Devine<sup>2,3</sup>, James Dibb<sup>2,3</sup>, David K. Edwards V<sup>1,2</sup>, Chris A. Eide<sup>2,3</sup>, Isabel English<sup>2,3</sup>, Jason Glover<sup>2,10</sup>, Rachel Henson<sup>2,8</sup>, Hiberny Ho<sup>2,3</sup>, Abdusebur Jemal<sup>2,10</sup>, Kara Johnson<sup>2,3</sup>, Ryan Johnson<sup>2,3</sup>, Brian Junio<sup>2,3</sup>, Andy Kaempf<sup>2,11</sup>, Jessica Leonard<sup>2,3</sup>, Chenwei Lin<sup>2,8</sup>, Selina (Qiuying) Liu<sup>2,3</sup>, Pierrette Lo<sup>2,3</sup>, Marc M. Loriaux<sup>2,12</sup>, Samuel Luty<sup>2,3</sup>, Tara Macey<sup>2,3</sup>, Jason MacManiman<sup>1,2</sup>, Jacqueline Martinez<sup>1,2</sup>, Motomi Mori<sup>2,11,13</sup>, Dylan Nelson<sup>14</sup>, Ceilidh Nichols<sup>2,3</sup>, Jill Peters<sup>2,3</sup>, Justin Ramsdill<sup>5,6</sup>, Angela Rofelty<sup>1,2</sup>, Robert Schuff<sup>5,6</sup>, Robert Searles<sup>2,8</sup>, Erik Segerdell<sup>2,5</sup>, Rebecca L. Smith<sup>2,3</sup>, Stephen E. Spurgeon<sup>2,3</sup>, Tyler Sweeney<sup>2,3</sup>, Aashis Thapa<sup>2,3</sup>, Corinne Visser<sup>2,3</sup>, Jake Wagner<sup>2,3</sup>, Kevin Watanabe-Smith<sup>2,3</sup>, Kristen Werth<sup>2,3</sup>, Joelle Wolf<sup>2,10</sup>, Libbey White<sup>2,5</sup>, Amy Yates<sup>5,6</sup>, Haijiao Zhang<sup>1,2</sup>, Christopher R. Cogle<sup>15</sup>, Robert H. Collins<sup>16</sup>, Denise C. Connolly<sup>17,18</sup>, Michael W. Deininger<sup>19</sup>, Leylah Drusbosky<sup>15</sup>, Christopher S. Hourigan<sup>20</sup>, Craig T. Jordan<sup>21</sup>, Patricia Kropf<sup>22</sup>, Tara L. Lin<sup>23</sup>, Micaela E. Martinez<sup>24</sup>, Bruno C. Medeiros<sup>25</sup>, Rachel R. Pallapati<sup>24</sup>, Daniel A. Pollyea<sup>21</sup>, Ronan T. Swords<sup>26</sup>, Justin M. Watts<sup>26</sup>, Scott J. Weir<sup>27,28</sup>, David L. Wiest<sup>29</sup>, Ryan M. Winters<sup>18</sup>, Shannon K. McWeeney<sup>2,5,6</sup>, and Brian J. Druker<sup>2,3,4</sup>

## Affiliations

<sup>1</sup>Department of Cell, Developmental & Cancer Biology, Oregon Health & Science University, Portland, OR

<sup>2</sup>Knight Cancer Institute, Oregon Health & Science University, Portland, OR

<sup>3</sup>Division of Hematology & Medical Oncology, Department of Medicine, Oregon Health & Science University, Portland, OR



- <sup>4</sup>Howard Hughes Medical Institute
- <sup>5</sup>Division of Bioinformatics and Computational Biology, Department of Medical Informatics and Clinical Epidemiology, Oregon Health & Science University, Portland, OR
- <sup>6</sup>Oregon Clinical & Translational Research Institute, Oregon Health & Science University, Portland, OR
- <sup>7</sup>Department of Molecular & Medical Genetics, Oregon Health & Science University, Portland, OR
- <sup>8</sup>Integrated Genomics Laboratories, Oregon Health & Science University, Portland, OR
- <sup>9</sup>Technology Transfer & Business Development, Oregon Health & Science University, Portland, OR
- <sup>10</sup>Division of Hematology and Oncology, Department of Pediatrics, Oregon Health & Science University, Portland, OR
- <sup>11</sup>Biostatistics Shared Resource, Oregon Health & Science University, Portland, OR
- <sup>12</sup>Department of Pathology, Oregon Health & Science University, Portland, OR
- <sup>13</sup>Oregon Health & Science University-Portland State University School of Public Health, Portland, OR
- <sup>14</sup>High-Throughput Screening Services Laboratory, Oregon State University, Corvallis, OR
- <sup>15</sup>Department of Medicine, Division of Hematology and Oncology, University of Florida, Gainesville, FL
- <sup>16</sup>Department of Internal Medicine/ Hematology Oncology, University of Texas Southwestern Medical Center, Dallas, TX
- <sup>17</sup>Molecular Therapeutics Program, Fox Chase Cancer Center, Philadelphia, PA
- <sup>18</sup>Fox Chase Cancer Center Biosample Repository Facility, Philadelphia, PA
- <sup>19</sup>Division of Hematology & Hematologic Malignancies, Department of Internal Medicine, University of Utah, Salt Lake City, UT
- <sup>20</sup>National Heart, Lung and Blood Institute, National Institutes of Health, Bethesda, MD
- <sup>21</sup>Division of Hematology, University of Colorado, Denver, CO
- <sup>22</sup>Bone Marrow Transplant Program, Fox Chase Cancer Center, Philadelphia, PA
- <sup>23</sup>Division of Hematologic Malignancies & Cellular Therapeutics, University of Kansas, Kansas City, KS
- <sup>24</sup>Clinical Research Services, University of Miami Sylvester Comprehensive Cancer Center, Miami, FL

<sup>25</sup>Department of Medicine – Hematology, Stanford University, Stanford, CA

<sup>26</sup>Department of Hematology, University of Miami Sylvester Comprehensive Cancer Center, Miami, FL

<sup>27</sup>Department of Toxicology, Pharmacology and Therapeutics, University of Kansas Medical Center, Kansas City, KS

<sup>28</sup>Department of Medicine, Division of Medical Oncology, University of Kansas Medical Center, Kansas City, KS

<sup>29</sup>Blood Cell Development and Function Program, Fox Chase Cancer Center, Philadelphia, PA

## Acknowledgements

We thank all of our patients at all sites for donating precious time and tissue. DNA and RNA quality assessments, library creation, and short read sequencing assays were performed by the OHSU Massively Parallel Sequencing Shared Resource. Sheenu Sheela, Catherine Lai, Katherine Lindblad and Kary Oetjen assisted in study coordination at NIH. Barry Sawicki and Christina Cline assisted in study coordination at the University of Florida. S. Ravencroft assisted with patient sample shipping and data entry and K. Schorno provided project management and support of activities at the University of Kansas Cancer Center. Jack Taw assisted with patient sample shipping and Shyam Patel assisted with data entry at Stanford University.

**Funding** Funding for this project was provided in part by a Leukemia Lymphoma Therapy Acceleration Grant to B.J.D. and J.W.T. and by support provided by the Knight Cancer Research Institute (Oregon Health & Science University, OHSU). Supported by grants from the National Cancer Institute (1U01CA217862, 1U54CA224019, 3P30CA069533–18S5) and NIH/NCATS CTSA UL1TR002369 (SKM, BW). ASB was supported by the National Library of Medicine Informatics Training Grant (T15LM007088). JWT received grants from the V Foundation for Cancer Research, the Gabrielle’s Angel Foundation for Cancer Research, and the National Cancer Institute (1R01CA183947). CRC received a Scholar in Clinical Research Award from The Leukemia & Lymphoma Society (2400–13), was distinguished with a Pierre Chagnon Professorship in Stem Cell Biology and Blood & Marrow Transplant and a UF Research Foundation Professorship. This work was supported in part by the Intramural Research Program of the National Heart, Lung, and Blood Institute of the National Institutes of Health.

The authors declare competing financial interests detailed below.

**Competing Interests** JWT receives research support from Agios, Aptose, Array, AstraZeneca, Constellation, Genentech, Gilead, Incyte, Janssen, Seattle Genetics, Syros, Takeda; JWT is a co-founder of Vivid Biosciences. MWD serves on the advisory boards and/or as a consultant for Novartis, Incyte, and BMS and receives research funding from BMS and Gilead. CSH receives research funding from Merck. TLL consults for Jazz Pharmaceuticals and receives research funding from Tolero, Gilead, Precient, Ono, Bio-Path, Mateon, Genentech/Roche, Trovogene, Abbvie, Pfizer, Celgene, Imago, Astellas, Karyopharm, Seattle Genetics, and Incyte. DAP receives research funding from Pfizer and Agios and served on advisory boards for Pfizer, Celyad, Agios, Celgene, AbbVie, Argenx, Takeda and Servier. BJD serves on the advisory boards for Gilead, Aptose, and Blueprint Medicines. BJD is principal investigator or coinvestigator on Novartis and BMS clinical trials. His institution, Oregon Health & Science University, has contracts with these companies to pay for patient costs, nurse and data manager salaries, and institutional overhead. He does not derive salary, nor does his laboratory receive funds from these contracts. The authors certify that all compounds tested in this study were chosen without input from any of our industry partners.

## REFERENCES

1. Jemal A, Siegel R, Xu J & Ward E Cancer statistics, 2010. *CA: a cancer journal for clinicians* 60, 277–300, (2010). [PubMed: 20610543]
2. National Cancer Institute: Surveillance, Epidemiology, and End Results Program, <<https://seer.cancer.gov/staffacts/html/amy1.html>> (2018).
3. Papaemmanuil E et al. Genomic Classification and Prognosis in Acute Myeloid Leukemia. *N Engl J Med* 374, 2209–2221, (2016). [PubMed: 27276561]
4. Arber DA et al. The 2016 revision to the World Health Organization classification of myeloid neoplasms and acute leukemia. *Blood* 127, 2391–2405, (2016). [PubMed: 27069254]



5. Dohner H et al. Diagnosis and management of AML in adults: 2017 ELN recommendations from an international expert panel. *Blood* 129, 424–447, (2017). [PubMed: 27895058]
6. TCGA. Genomic and epigenomic landscapes of adult de novo acute myeloid leukemia. *N Engl J Med* 368, 2059–2074, (2013). [PubMed: 23634996]
7. Byrd JC et al. Pretreatment cytogenetic abnormalities are predictive of induction success, cumulative incidence of relapse, and overall survival in adult patients with de novo acute myeloid leukemia: results from Cancer and Leukemia Group B (CALGB 8461). *Blood* 100, 4325–4336, (2002). [PubMed: 12393746]
8. Patel JP et al. Prognostic relevance of integrated genetic profiling in acute myeloid leukemia. *N Engl J Med* 366, 1079–1089, (2012). [PubMed: 22417203]
9. Haferlach T et al. Landscape of genetic lesions in 944 patients with myelodysplastic syndromes. *Leukemia* 28, 241–247, (2014). [PubMed: 24220272]
10. Lundberg P et al. Clonal evolution and clinical correlates of somatic mutations in myeloproliferative neoplasms. *Blood* 123, 2220–2228, (2014). [PubMed: 24478400]
11. Deininger MWN, Tyner JW & Solary E Turning the tide in myelodysplastic/myeloproliferative neoplasms. *Nat Rev Cancer* 17, 425–440, (2017).
12. Busque L et al. Recurrent somatic TET2 mutations in normal elderly individuals with clonal hematopoiesis. *Nat Genet* 44, 1179–1181, (2012). [PubMed: 23001125]
13. Genovese G et al. Clonal hematopoiesis and blood-cancer risk inferred from blood DNA sequence. *N Engl J Med* 371, 2477–2487, (2014). [PubMed: 25426838]
14. Jaiswal S et al. Age-related clonal hematopoiesis associated with adverse outcomes. *N Engl J Med* 371, 2488–2498, (2014). [PubMed: 25426837]
15. Xie M et al. Age-related mutations associated with clonal hematopoietic expansion and malignancies. *Nat Med* 20, 1472–1478, (2014). [PubMed: 25326804]
16. Huang ME et al. Use of all-trans retinoic acid in the treatment of acute promyelocytic leukemia. *Blood* 72, 567–572, (1988). [PubMed: 3165295]
17. Shen ZX et al. Use of arsenic trioxide (As<sub>2</sub>O<sub>3</sub>) in the treatment of acute promyelocytic leukemia (APL): II. Clinical efficacy and pharmacokinetics in relapsed patients. *Blood* 89, 3354–3360, (1997). [PubMed: 9129042]
18. Nakao M et al. Internal tandem duplication of the *flt3* gene found in acute myeloid leukemia. *Leukemia* 10, 1911–1918, (1996). [PubMed: 8946930]
19. Tse KF, Mukherjee G & Small D Constitutive activation of FLT3 stimulates multiple intracellular signal transducers and results in transformation. *Leukemia* 14, 1766–1776, (2000). [PubMed: 11021752]
20. Yamamoto Y et al. Activating mutation of D835 within the activation loop of FLT3 in human hematologic malignancies. *Blood* 97, 2434–2439, (2001). [PubMed: 11290608]
21. Yokota S et al. Internal tandem duplication of the FLT3 gene is preferentially seen in acute myeloid leukemia and myelodysplastic syndrome among various hematological malignancies. A study on a large series of patients and cell lines. *Leukemia* 11, 1605–1609, (1997). [PubMed: 9324277]
22. Knapper S et al. A phase 2 trial of the FLT3 inhibitor lestaurinib (CEP701) as first-line treatment for older patients with acute myeloid leukemia not considered fit for intensive chemotherapy. *Blood* 108, 3262–3270, (2006). [PubMed: 16857985]
23. O’Farrell AM et al. An innovative phase I clinical study demonstrates inhibition of FLT3 phosphorylation by SU11248 in acute myeloid leukemia patients. *Clin Cancer Res* 9, 5465–5476, (2003). [PubMed: 14654525]
24. Smith BD et al. Single-agent CEP-701, a novel FLT3 inhibitor, shows biologic and clinical activity in patients with relapsed or refractory acute myeloid leukemia. *Blood* 103, 3669–3676, (2004). [PubMed: 14726387]
25. DeAngelo DJ et al. Phase I clinical results with tandutinib (MLN518), a novel FLT3 antagonist, in patients with acute myelogenous leukemia or high-risk myelodysplastic syndrome: safety, pharmacokinetics, and pharmacodynamics. *Blood* 108, 3674–3681, (2006). [PubMed: 16902153]
26. Stone RM et al. Midostaurin plus Chemotherapy for Acute Myeloid Leukemia with a FLT3 Mutation. *N Engl J Med* 377, 454–464, (2017). [PubMed: 28644114]

27. Mardis ER et al. Recurring mutations found by sequencing an acute myeloid leukemia genome. *N Engl J Med* 361, 1058–1066, (2009). [PubMed: 19657110]
28. Wang F et al. Targeted inhibition of mutant IDH2 in leukemia cells induces cellular differentiation. *Science* 340, 622–626, (2013). [PubMed: 23558173]
29. Rohle D et al. An inhibitor of mutant IDH1 delays growth and promotes differentiation of glioma cells. *Science* 340, 626–630, (2013). [PubMed: 23558169]
30. Fiskus W et al. Combined epigenetic therapy with the histone methyltransferase EZH2 inhibitor 3-deazaneplanocin A and the histone deacetylase inhibitor panobinostat against human AML cells. *Blood* 114, 2733–2743, (2009). [PubMed: 19638619]
31. Schenk T et al. Inhibition of the LSD1 (KDM1A) demethylase reactivates the all-trans-retinoic acid differentiation pathway in acute myeloid leukemia. *Nat Med* 18, 605–611, (2012). [PubMed: 22406747]
32. Daigle SR et al. Selective killing of mixed lineage leukemia cells by a potent small-molecule DOT1L inhibitor. *Cancer Cell* 20, 53–65, (2011). [PubMed: 21741596]
33. Itzykson R et al. Impact of TET2 mutations on response rate to azacitidine in myelodysplastic syndromes and low blast count acute myeloid leukemias. *Leukemia* 25, 1147–1152, (2011). [PubMed: 21494260]
34. Welch JS et al. TP53 and Decitabine in Acute Myeloid Leukemia and Myelodysplastic Syndromes. *N Engl J Med* 375, 2023–2036, (2016). [PubMed: 27959731]
35. Konopleva M et al. Efficacy and Biological Correlates of Response in a Phase II Study of Venetoclax Monotherapy in Patients with Acute Myelogenous Leukemia. *Cancer Discov* 6, 1106–1117, (2016). [PubMed: 27520294]
36. DiNardo CD et al. Safety and preliminary efficacy of venetoclax with decitabine or azacitidine in elderly patients with previously untreated acute myeloid leukaemia: a non-randomised, open-label, phase 1b study. *Lancet Oncol*, (2018).
37. Tyner JW et al. Kinase Pathway Dependence in Primary Human Leukemias Determined by Rapid Inhibitor Screening. *Cancer Res* 73, 285–296, (2013). [PubMed: 23087056]
38. Benjamini Y & Hochberg Y Controlling the false discovery rate: A practical and powerful approach to multiple testing. *Journal of the Royal Statistical Society, Series B (Methodological)* 57, 289–300, (1995).
39. Puissant A et al. SYK is a critical regulator of FLT3 in acute myeloid leukemia. *Cancer Cell* 25, 226–242, (2014). [PubMed: 24525236]
40. Canisius S, Martens JWM & Wessels LFA A novel independence test for somatic alterations in cancer shows that biology drives mutual exclusivity but chance explains most co-occurrence. *Genome biology* 17, 261, (2016). [PubMed: 27986087]
41. Li H & Durbin R Fast and accurate short read alignment with Burrows-Wheeler transform. *Bioinformatics* 25, 1754–1760, (2009). [PubMed: 19451168]
42. McKenna A et al. The Genome Analysis Toolkit: a MapReduce framework for analyzing next-generation DNA sequencing data. *Genome Res* 20, 1297–1303, (2010). [PubMed: 20644199]
43. Huntley MA et al. ReportingTools: an automated result processing and presentation toolkit for high-throughput genomic analyses. *Bioinformatics* 29, 3220–3221, (2013). [PubMed: 24078713]
44. Buffalo V qrqc: Quick Read Quality Control. R package version 1.22.0, <http://github.com/vsbuffalo/qrc>. (2012).
45. Cibulskis K et al. Sensitive detection of somatic point mutations in impure and heterogeneous cancer samples. *Nat Biotechnol* 31, 213–219, (2013). [PubMed: 23396013]
46. Koboldt DC et al. VarScan 2: somatic mutation and copy number alteration discovery in cancer by exome sequencing. *Genome Res* 22, 568–576, (2012). [PubMed: 22300766]
47. McLaren W et al. Deriving the consequences of genomic variants with the Ensembl API and SNP Effect Predictor. *Bioinformatics* 26, 2069–2070, (2010). [PubMed: 20562413]
48. Kandoth, C. <https://github.com/ckandoth/vcf2maf>.
49. varscan: Variant calling and somatic mutation/CNV detection for next-generation sequencing data (2018).

50. vcf2maf: Convert a VCF into a MAF, where each variant is annotated to only one of all possible gene isoforms (Memorial Sloan Kettering, 2018).
51. Zhao H et al. CrossMap: a versatile tool for coordinate conversion between genome assemblies. *Bioinformatics* 30, 1006–1007, (2014). [PubMed: 24351709]
52. Lek M et al. Analysis of protein-coding genetic variation in 60,706 humans. *Nature* 536, 285–291, (2016). [PubMed: 27535533]
53. Ye K, Schulz MH, Long Q, Apweiler R & Ning Z Pindel: a pattern growth approach to detect break points of large deletions and medium sized insertions from paired-end short reads. *Bioinformatics* 25, 2865–2871, (2009). [PubMed: 19561018]
54. Costello M et al. Discovery and characterization of artifactual mutations in deep coverage targeted capture sequencing data due to oxidative DNA damage during sample preparation. *Nucleic Acids Research* 41, e67, (2013). [PubMed: 23303777]
55. Kottaridis PD et al. The presence of a FLT3 internal tandem duplication in patients with acute myeloid leukemia (AML) adds important prognostic information to cytogenetic risk group and response to the first cycle of chemotherapy: analysis of 854 patients from the United Kingdom Medical Research Council AML 10 and 12 trials. *Blood* 98, 1752–1759, (2001). [PubMed: 11535508]
56. Dohner K et al. Mutant nucleophosmin (NPM1) predicts favorable prognosis in younger adults with acute myeloid leukemia and normal cytogenetics: interaction with other gene mutations. *Blood* 106, 3740–3746, (2005). [PubMed: 16051734]
57. Falini B, Nicoletti I, Martelli MF & Mecucci C Acute myeloid leukemia carrying cytoplasmic/mutated nucleophosmin (NPMc+ AML): biologic and clinical features. *Blood* 109, 874–885, (2007). [PubMed: 17008539]
58. Huang Q et al. A rapid, one step assay for simultaneous detection of FLT3/ITD and NPM1 mutations in AML with normal cytogenetics. *Br J Haematol* 142, 489–492, (2008). [PubMed: 18477048]
59. Wouters BJ et al. Double CEBPA mutations, but not single CEBPA mutations, define a subgroup of acute myeloid leukemia with a distinctive gene expression profile that is uniquely associated with a favorable outcome. *Blood* 113, 3088–3091, (2009). [PubMed: 19171880]
60. Liao Y, Smyth GK & Shi W The Subread aligner: fast, accurate and scalable read mapping by seed-and-vote. *Nucleic Acids Res* 41, e108, (2013). [PubMed: 23558742]
61. Liao Y, Smyth GK & Shi W featureCounts: an efficient general purpose program for assigning sequence reads to genomic features. *Bioinformatics* 30, 923–930, (2014). [PubMed: 24227677]
62. Langfelder P & Horvath S WGCNA: an R package for weighted correlation network analysis. *BMC bioinformatics* 9, 559, (2008). [PubMed: 19114008]
63. Hansen KD, Irizarry RA & Wu Z Removing technical variability in RNA-seq data using conditional quantile normalization. *Biostatistics* 13, 204–216, (2012). [PubMed: 22285995]
64. Kim D & Salzberg SL TopHat-Fusion: an algorithm for discovery of novel fusion transcripts. *Genome biology* 12, R72, (2011). [PubMed: 21835007]
65. Langfelder P & Horvath S Fast R Functions for Robust Correlations and Hierarchical Clustering. *Journal of Statistical Software* 46, (2012).
66. Langfelder P, Luo R, Oldham MC & Horvath S Is My Network Module Preserved and Reproducible? *PLoS computational biology* 7, e1001057, (2011). [PubMed: 21283776]
67. Parsana P et al. Addressing confounding artifacts in reconstruction of gene co-expression networks. *bioRxiv*, 202903, (2017).
68. Zheng X et al. A high-performance computing toolset for relatedness and principal component analysis of SNP data. *Bioinformatics* 28, 3326–3328, (2012). [PubMed: 23060615]
69. International HapMap C The International HapMap Project. *Nature* 426, 789–796, (2003). [PubMed: 14685227]
70. Zheng X & Weir BS Eigenanalysis of SNP data with an identity by descent interpretation. *Theoretical Population Biology* 107, 65–76, (2016). [PubMed: 26482676]
71. Robinson MD & Oshlack A A scaling normalization method for differential expression analysis of RNA-seq data. *Genome biology* 11, R25, (2010). [PubMed: 20196867]

72. Slovak ML, Theisen A & Shaffer LG in *The Principles of Clinical Cytogenetics* (eds Gersen Steven L. & Keagle Martha B.) 23–49 (Springer New York, 2013).
73. Kurtz SE et al. Molecularly targeted drug combinations demonstrate selective effectiveness for myeloid- and lymphoid-derived hematologic malignancies. *Proc Natl Acad Sci U S A* 114, E7554–E7563, (2017). [PubMed: 28784769]
74. Davis MI et al. Comprehensive analysis of kinase inhibitor selectivity. *Nat Biotechnol* 29, 1046–1051, (2011). [PubMed: 22037378]
75. Blucher AS, Choonoo G, Kulesz-Martin M, Wu G & McWeeney SK Evidence-Based Precision Oncology with the Cancer Targetome. *Trends in pharmacological sciences* 38, 1085–1099, (2017). [PubMed: 28964549]
76. Gu Z, Eils R & Schlesner M Complex heatmaps reveal patterns and correlations in multidimensional genomic data. *Bioinformatics* 32, 2847–2849, (2016). [PubMed: 27207943]
77. Ritchie ME et al. limma powers differential expression analyses for RNA-sequencing and microarray studies. *Nucleic Acids Research* 43, e47–e47, (2015). [PubMed: 25605792]
78. Leek JT & Storey JD Capturing Heterogeneity in Gene Expression Studies by Surrogate Variable Analysis. *PLOS Genetics* 3, e161, (2007).
79. Law CW, Chen Y, Shi W & Smyth GK voom: precision weights unlock linear model analysis tools for RNA-seq read counts. *Genome biology* 15, R29, (2014). [PubMed: 24485249]
80. Parker HS, Bravo HC & Leek JT Removing batch effects for prediction problems with frozen surrogate variable analysis. *PeerJ* 2, e561, (2014). [PubMed: 25332844]
81. Fraley C & Raftery AE Enhanced Model-Based Clustering, Density Estimation, and Discriminant Analysis Software: MCLUST. *Journal of Classification* 20, 263–286, (2003).
82. Pison G, Struyf A & Rousseeuw PJ Displaying a clustering with CLUSPLOT. *Computational Statistics & Data Analysis* 30, 381–392, (1999).
83. Package corrplot is for visualizing a correlation matrix (2018).
84. Tibshirani R Regression Shrinkage and Selection via the Lasso. *Journal of the Royal Statistical Society. Series B (Methodological)* 58, 267–288, (1996).
85. Friedman J, Hastie T & Tibshirani R Regularization Paths for Generalized Linear Models via Coordinate Descent. *Journal of Statistical Software* 33, (2010).
86. Iorio F et al. A Landscape of Pharmacogenomic Interactions in Cancer. *Cell* 166, 740–754, (2016). [PubMed: 27397505]

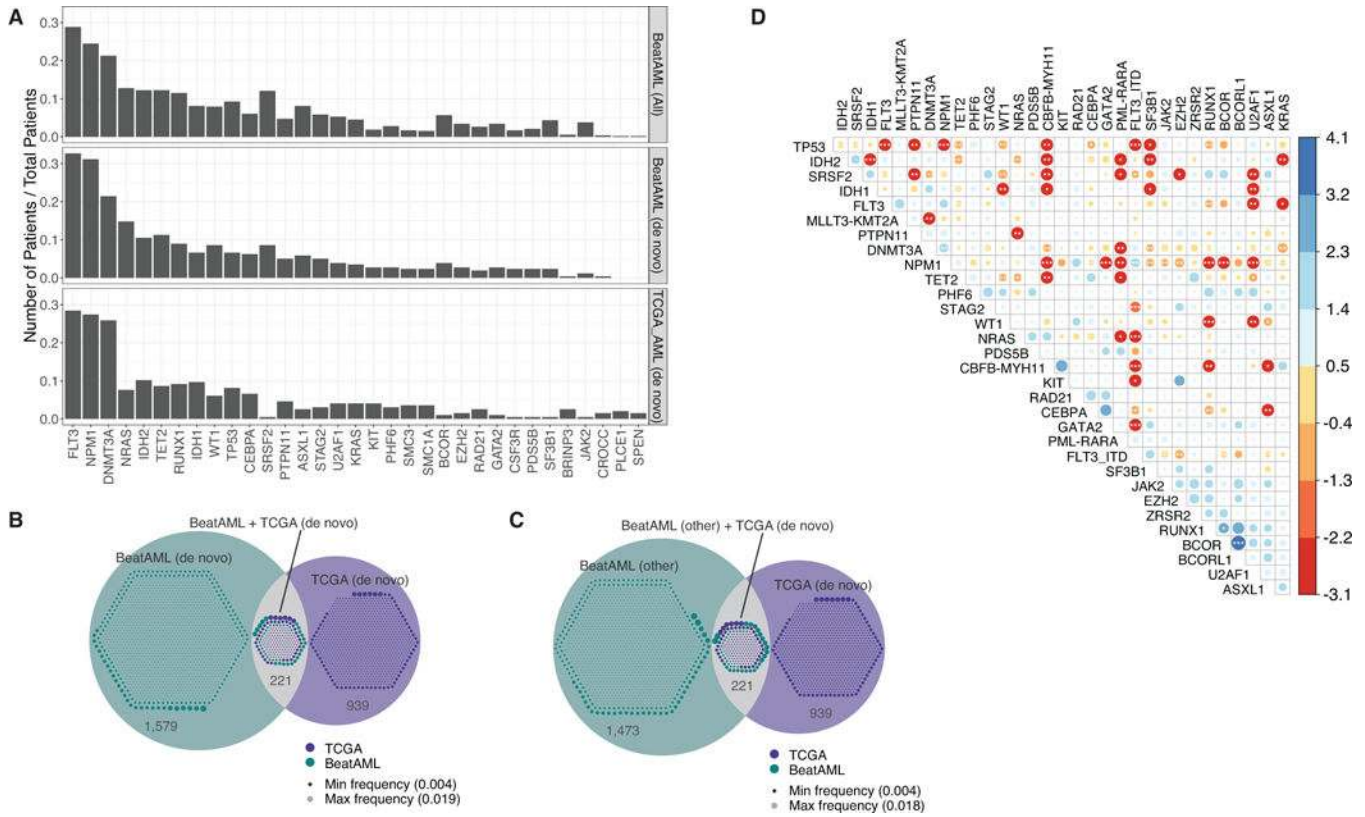


**Fig. 1. Comparative Genomic Landscape of AML.**

(A) Frequency of the 33 mutational events that were cumulatively most frequent in Beat AML (n=531 patients) and TCGA (n=200 patients). Top row represents the full Beat AML cohort and the middle bar represents only the *de novo* Beat AML cases. Mutations were summarized by gene as was done by TCGA whereas the FLT3-ITD mutations were kept separate in the rest of this manuscript.

(B) Mutational events at 2% frequency or less in the *de novo* cases of Beat AML and TCGA were compared for overlap. Venn diagram displays the overlap with the small circles within each compartment representing a size-scaled frequency of each mutational event.

(C) Analysis as in panel B with only the non-*de novo* Beat AML cases versus TCGA.

(D) Co-occurrence or exclusivity of the most recurrent mutational events in the Beat AML cohort (n=531 patients) were assessed using the DISCOVER<sup>40</sup> method with a dot plot indicating the odds ratio of co-occurrence (blue) or exclusivity (red) using color-coding and circle size as well as asterisks that indicate FDR-corrected statistical significance.



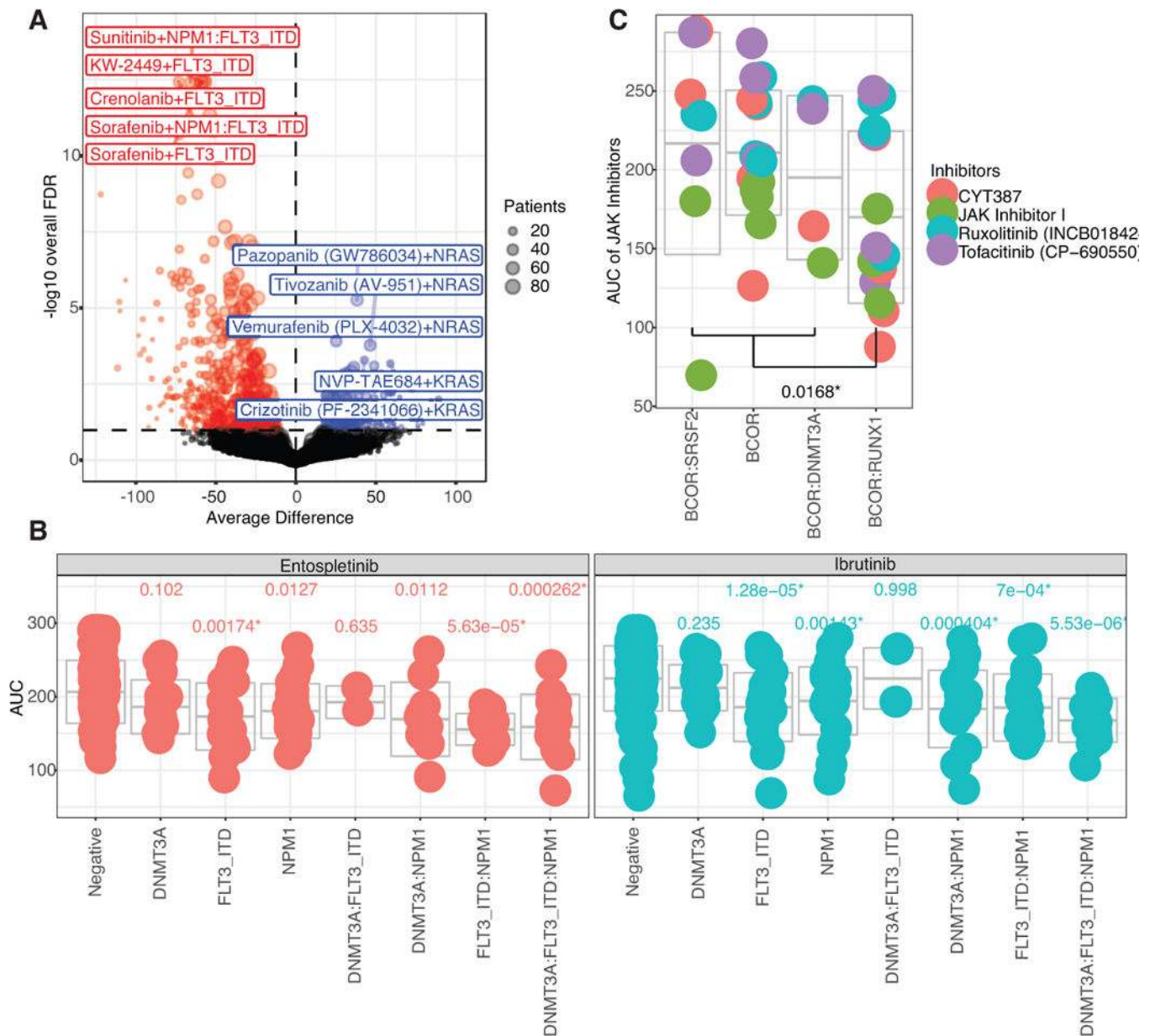


**Fig. 2. Integration of Genetic Events with Drug Sensitivity.**

(A) Average difference in AUC drug response between mutant and wild type cases was determined using a two-sided t-test from a linear model fit (plotted on the horizontal axis and FDR-corrected q-value is plotted on the vertical axis). FDR was computed using the Benjamini-Hochberg (BH) over all the drugs. The n used to correlate each mutational event with drug sensitivity is reported in the Supplementary Information (Table S17). Expanded and interactive plots are available in our online data browser ([www.vizome.org](http://www.vizome.org)) and ([http://vizome.org/additional\\_figures\\_BeatAML.html](http://vizome.org/additional_figures_BeatAML.html)).

(B) Area under the curve for ibrutinib or entospletinib (n=277 or 168 patient samples, respectively) was plotted for cases with single, double, or triple mutation of FLT3-ITD, NPM1, and DNMT3A with the mean and one s.d. indicated by center and outer gray bars,



respectively. An ANOVA was conducted using the Bonferroni approach (statistical results and sample size for all groups reported in Supplementary Information, Tables S18,19). (C) Inhibitors of JAK family kinases were assessed for activity against cases with BCOR mutation alone or BCOR in combination with SRSF2, RUNX1, or DNMT3A. The AUC values are plotted per case with the mean and one standard deviation indicated by center and outer gray bars, respectively. There was a significant difference in AUC by two-sided t-test ( $t(42)=-2.489$ ,  $p=0.0168$ , 95% CI [-73.018, -7.643]) between BCOR and RUNX1 (n=16) versus the average of BCOR alone (n=16), BCOR and SRSF2 (n=8), and BCOR and DNMT3A (n=4).

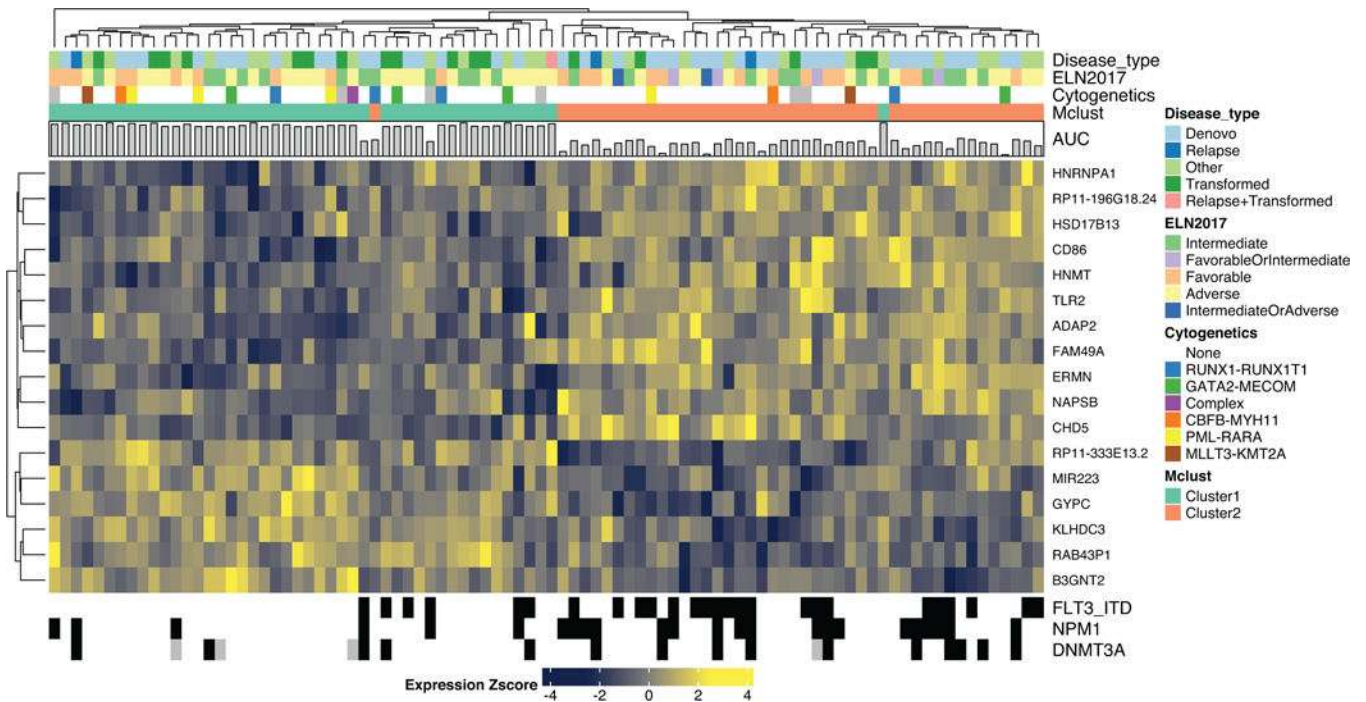


**Fig. 3. Integration of Gene Expression and Drug Sensitivity Patterns.**

Differential gene expression signature distinguishing the 20% most ibrutinib sensitive (n=46) from 20% most resistant (n=44) specimens. Heatmaps for all other drugs are available in our online data browser ([http://vizome.org/additional\\_figures\\_BeatAML.html](http://vizome.org/additional_figures_BeatAML.html)). For the n used to correlate each drug with gene expression, please see Supplementary Information (Table S17).